NONLINEAR EVOLUTION OF THE INTERFACE BETWEEN TWO IMMISCIBLE FLUIDS IN A MICRO CHANNEL SUBJECTED TO AN ELECTRIC FIELD

by

Suat Canberk Ozan

B.S., Chemical Engineering, Boğaziçi University, 2014

Submitted to the Institute for Graduate Studies in
Science and Engineering in partial fulfillment of
the requirements for the degree of
Master of Science

Graduate Program in Chemical Engineering

Boğaziçi University

2016

ACKNOWLEDGEMENTS

First of all, I would like to thank my thesis supervisor Assoc. Prof. A. Kerem Uğuz for his support, guidance and motivation throughout the research.

Besides, I am grateful to the jury members Prof. Ramazan Yıldırım and Prof. Metin Muradoğlu for their time and consideration.

I am very grateful to members of KB 406 Pınar Eribol and Sercan Altundemir for their friendship and support. If it wasn't for them it would have been quite difficult to conduct this study without getting bored in the laboratory.

Also, I want to thank Pelin Su Bulutoğlu, Begüm Koca and Tugçe İr for always being there, and always supporting and motivating me. They have never left me alone during the difficult times of this research.

I acknowledge all help from my professors, my teaching assistant friends and supporting personnel of chemical engineering department, especially from Melike Gürbüz.

Finally, I want to thank my close friends Mustafa Ercan and Barış Süslü, and my family, especially my sister Ece Ozan. Although we could only rarely have the chance to meet throughout the last year, I knew that they were always there for me.

I also acknowledge the financial support provided by Boğaziçi University Research Fund Grant Number 11521.

ABSTRACT

NONLINEAR EVOLUTION OF THE INTERFACE BETWEEN TWO IMMISCIBLE FLUIDS IN A MICRO CHANNEL SUBJECTED TO AN ELECTRIC FIELD

In this work, the nonlinear evolution of the interface between two immiscible, Newtonian, leaky dielectric fluids in a micro channel subjected to a pressure-driven base flow in the presence of an electric field applied normal to the interface is investigated. The long wave analysis of the interface is performed and the evolution equations of the interface position and the surface charge density are derived. The evolution equations are solved using a numerical procedure, in which the Fourier transform and the 4^{th} order Runge-Kutta formulation are used to discretize the space and the time derivatives, respectively. A major result indicates that the presence of a pressure-driven base flow prevents the interface from reaching the walls of the channel and also results in loss of symmetry of the interface. Stronger base flow reduces the vertical distance between the maximum and the minimum of the interface, i.e. the amplitude of the interface. As linear theory suggests, the early times of the evolution of the interface do not depend on the presence or the strength of the base flow. In addition to the base flow analysis, a parametric study, which involves the depth, the viscosity and the conductivity ratios, and the dimensionless groups, namely the electric number and the ratio of the fluid to electric time scales, is conducted. It is revealed that increasing the electric number leads to a more symmetrical interface position profile with a larger amplitude, which means that it has the exact opposite effect on the interface compared to the strength of the base flow. The parametric study also shows that when the viscosity ratio is constant, the largest interface amplitude occurs for the depth ratio that gives a base state velocity profile, for which the maximum is at the flat interface between the fluids.

ÖZET

BİR MİKRO KANALDA AKMAKTA OLAN KARIŞMAYAN İKİ AKIŞKANIN ARAYÜZEYİNİN ELEKTRİK ALAN ETKİSİNDE LİNEER OLMAYAN GELİŞİMİ

Bu çalışmada, bir mikro kanalda basınç farkı sebebiyle akmakta olan karışmayan iki Newtonyen yarı iletken akışkanın arasındaki arayüzeyin doğrusal olmayan gelişimi, arayüzeye dik olarak uygulanan bir elektrik alanının varlığında incelenmektedir. Arayüzey pozisyonu ve yüzey yük yoğunluğu için gelişim denklemleri uzun dalga analizi kullanılarak elde edilmektedir. Gelişim denklemleri, zaman ve pozisyon türevleri için sırasıyla Fourier dönüşümü ve 4. derece Runge-Kutta formülasyonu kullanan bir nümerik yöntemle çözülmektedir. Sonuçlar, basınca dayalı akışın, arayüzeyin kanal duvarlarına ulaşmasını engellediğini ve aynı zamanda arayüzeyde simetrinin yok olmasına sebep olduğunu göstermektedir. Akışın kuvvetlenmesi arayüzeyin maksimum ve minimumu arasındaki dikey farkın, bir başka deyişle arayüzeyin genliğinin azalmasına sebep olmaktadır. Lineer teorinin gösterdiği gibi arayüzeyin gelişimi ilk zamanlarında akışın varlığından ya da kuvvetinden etkilenmemektedir. Akışın etkisine ek olarak derinlik, viskozite ve iletkenlik oranlarını, ve boyutsuz sayılar olan elektrik sayısını ve akışkan zaman ölçeğinin elektrik zaman ölçeğine oranını içeren bir parametrik çalışma yapılmaktadır. Elektrik sayısını arttırmak akışın kuvvetini arttırmanın tam aksine daha yüksek genlikli ve daha simetrik arayüzeylerin gözlemlenmesine sebep olmaktadır. Parametrik çalışma aynı zamanda viskozite oranı sabitken en büyük arayüzey genliğine, hız profilinin maksimumu düz arayüzeyde olduğunda ulaşıldığını ortaya çıkarmaktadır.

TABLE OF CONTENTS

LIST OF FIGURES

LIST OF SYMBOLS

A	Amplitude of the initial disturbance
B	Wavenumber
Ca	Capillary number
d	Depth of the fluid
Eb	Electric number
$\underline{E}$	Electric field
f	An arbitrary function
$\underline{\underline{I}}$	Identity tensor
i	Imaginary unit
k	Eigenvalues of the Fourier derivative matrix
L	Length of the channel
$\underline{n}$	Unit normal vector
p	Pressure
q	Surface charge density
Re	Reynold number
S	Ratio of fluid to electric time scales
$\underline{\underline{T}}$	Total stress tensor
$\underline{\underline{T}}^E$	Electric component of the total stress tensor
$\underline{\underline{T}}^F$	Fluid component of the total stress tensor
$\underline{t}$	Unit tangent vector
U	Interface speed
u	x-component of the velocity field
$\underline{u}$	Interface velocity
u_{mult}	Multiplier of the velocity
V	Voltage field
V_b	Applied voltage
$\underline{v}$	Velocity field
w	z-component of the velocity field

Z	Interface position
α	Conductivity ratio
β	Depth ratio
γ	Interfacial tension
Δt	Time step size
ϵ	Ratio of the depth of the fluid to the length of the channel
ε	Electrical permittivity
ε_0	Electrical permittivity of vacuum
λ	Viscosity ratio
μ	Viscosity
ρ	Density
σ	Electrical conductivity
ϕ	Density ratio
∇	Gradient
∇_s	Surface divergence
$2H$	Twice of the mean curvature
$x^\star$	Property of the starred fluid
$\tilde{x}$	Scaled variable
$\hat{x}$	Perturbed variable
x_0	Base state variable
$\underline{x}^T$	Transpose of a vector
$F(x)$	Fourier transform of x
$F^{-1}(x)$	Inverse Fourier transform of x

LIST OF ACRONYMS/ABBREVIATIONS

AC	Alternating Current
DC	Direct Current
EHD	Electrohydrodynamic
LISA	Lithographically-Induced Self-Assembly

1. INTRODUCTION

Microfluidics is the branch of fluid mechanics, with typical dimensions on the order of microns up to 1mm. Recently, due to its numerous advantages, such as the usage of small sample sizes and short experimental times, microfluidics has gained more attraction from academia and industry [1]. Although microfluidics has several benefits, it also has some major drawbacks, such as difficulties in mixing. Since the length scales of microfluidic devices are small, the Reynolds number Re is also small; hence the flow is laminar [1]. As a consequence of the laminar flow regime, no turbulence is observed in the channel and mixing can only be achieved via molecular diffusion. Due to the small scales, the conventional mixing techniques, which are applied for large volumes, are not suitable for micro channels [2–4]. To achieve mixing, passive methods [5–7], which are based on complex channel geometries, and active methods [8–10], which employ external inputs such as electric or magnetic fields, or acoustics are used [11]. When two or more immiscible liquids are used in a micro channel, it is possible to form micro droplets of one liquid in a continuous phase by disturbing the interface between the liquids. Again, the methods which are used to form micro droplets are categorized as the passive and the active methods. The passive methods include different techniques based on the channel geometry such as co-flowing streams [12], T-shaped junctions [13] and flow focusing [14]. The active methods are based on external forces such as electric field [15], magnetic field [16], temperature [17] and pressure [18]. In this work, the focus is on the electric field. Depending on the magnitude of the voltage difference, applying an electric field on the fluids can deflect the interface between these immiscible fluids, which is a mechanism of an instability called electrohydrodynamic (EHD) instability [19, 20]. The reason behind an EHD instability is the discontinuities in the electrical conductivities and the permittivities of the fluids [21]. Application of a normal electric field to a polymer-air interface yields similar patterns [22, 23] to those that emerge in the lithographically-induced self-assembly (LISA) [24] process. Hence EHD instabilities have drawn more attention recently.

Different approaches are used to analyse EHD instabilities. The bulk-coupled model, used for miscible fluids, assumes the electrical forces on the fluid elements emerge as a result of the deviations in the conductivity in a thin diffusion layer between the fluids [25–27]. On the other hand, the surface coupled model is used for immiscible fluids. In the surface coupled model, the electrical terms appear only at the interface conditions and the model assumes jumps in the electrical properties of the fluids at the interface. [19, 21, 28–33]. Another classification of the models is based on the type of the fluid; the fluids are assumed to be either perfect dielectric [34, 35], where free charges in the fluid are absent and the electric field emerges due to polarization, or leaky dielectric [36, 37], where the conductivity is uniform and the free charge carriers are present, or conductive. The linear stability analyses show that the electric field is always destabilizing for perfect dielectrics [21, 38], whereas it can be stabilizing or destabilizing for leaky dielectrics depending on the parameters [21, 31, 32]. An overall result for the linear stability analysis is given by [33] including the permittivity and conductivity ratios and the direction of the electric field, which is applied either parallel or normal to the flat interface between the fluids.

The aim of this work is to examine the evolution of the interface between two immiscible, Newtonian and leaky dielectric fluids in a micro channel subjected to a pressure driven flow in the presence of an electric field applied normal to the flat interface. The fluids are allowed to have different viscosities, densities, electrical conductivities and permittivities. The nonlinear evolution equations for the interface position and the surface charge density are derived using the lubrication theory. A brief survey on the literature is presented in Section 2. In Section 3, the physical system is depicted and the key steps of the derivation of the mathematical model are given. The numerical procedure employed to solve the evolution equations and its validation are presented in Section 4.1 and Section 4.2, respectively. The effects of the base flow and the dimensionless parameters on the interface position and the surface charge density are given in Sections 4.3-4.8. In Section 5, conclusions and recommendations are given. The details of the derivation are given in the Appendix A.

2. LITERATURE SURVEY

In this section, a brief literature-survey on the electrohydrodynamic (EHD) instability is presented. EHD instability is an instability mechanism that stems from the discontinuities in the electrical conductivities and the permittivities of the fluids. An electric field that is applied to the interface between these fluids may deflect the interface depending on the magnitude of the electric field [19,20]. Most of the works in the literature on the subject are theoretical studies. Therefore the focus of the Section 2 is on theoretical studies. In a closely related experimental work, Eribol and Uguz [39] determine the critical voltage, which deflects the interface between two immiscible fluids subjected to a base pressure-driven flow in the presence of a DC electric field either normal or parallel to the flat interface. A parametric study in [39] show the critical voltage is only affected by the flow rate ratios, not by the individual flow rates.

In this work a surface coupled model, in which fluids are assumed to be leaky dielectrics is used. A direct current (DC) electric field is applied initially normal to the interface. The nonlinear governing equations with the interface and boundary conditions are solved to observe the behavior of the interface position. To distinguish the theoretical studies in the literature five criteria are selected. In Section 2.1 the first classification is made based on the coupling of the electrical terms and the hydrodynamic equations, and the works that employ the bulk coupled model are given in detail. In Sections 2.2-2.4 only the surface coupled model is considered. The second classification presented in Section 2.2 is made based on the type of the fluid in terms of its conductivity. The works, in which only perfect dielectrics or conductors are presented and the details for other works, i.e. the works with a surface coupled model and leaky dielectric fluids, are classified and summarized further in Sections 2.3 and 2.4. Two different characteristics are investigated in Section 2.3 and classifications based on the direction of the electric field and on the type of the current, i.e. alternating or direct currents, are made. The final classification is done in Section 2.4 based on the analysis method. A classification based on the type or presence of the base flow is not made, but the type of the flow is mentioned throughout Section 2 when it is present.

2.1. Bulk and Surface Coupled Models

Depending on the miscibility of the fluids, two different mathematical models are employed to investigate the EHD instability of the interface between the fluids. The models are classified in terms of the coupling of the electrical terms with the hydrodynamic equations. First one is the bulk coupled model, which is used to derive the EHD equations for miscible fluids [25–27]. According to the model, there are no jumps in the electrical properties across the interface and there is a conductivity gradient. The electrical forces on the fluid elements are caused by the deviations in the conductivity in a thin diffusion layer between the fluids [25–27]. In this model, the electrical forces are treated as body forces and included in the momentum balance equations. The first works on the EHD instabilities are presented by Hoburg and Melcher [26, 40]. Baygents and Baldessari [41] employed the bulk coupled model for a one-fluid system, which has a linear electrical conductivity profile, and conducted a linear stability analysis. It is possible to achieve rapid mixing due to the EHD instability; therefore, more recently, the model is used in studies that aim to overcome the problem of mixing in micro scale devices [42, 43]. This type of EHD instability is studied in different geometries such as a long rectangular shaped channel [3] or a cross-shaped junction [44]. A review of the works that employ the bulk coupled model and the EHD equations derived using the bulk coupled model are given by Lin [45].

Second model, which is also used in this work, is the surface coupled model. This model is widely used for the interfacial instabilities of immiscible fluids in the presence of an electric field [19, 21, 28–33]. Unlike the bulk coupled model, the surface coupled model assumes a jump in the electrical properties of the fluids at the interface. It also assumes that the free charges accumulate at the interface and the bulks of the fluids do not contain free charges. Therefore, the electrical terms do not appear in the governing equations and are only present at the interface conditions. The works reviewed in Sections 2.2-2.4 focus on the immiscible fluids and as thus the surface coupled model is employed in them. Therefore, to avoid repetition the details of those works are not given here.

2.2. Fluid Conductivity Models

The models in the literature are also classified based on the type of the conductivity of the fluids. Two extremes in terms of electrical conductivity are the perfect dielectric and conductor models, in which the fluid is non-conducting and perfectly conducting, respectively. The third model, namely the leaky dielectric model is proposed by Taylor [36, 37] to represent the behavior of a poorly conducting fluid and used by Melcher to develop electrohydrodynamics [37]. The model assumes a uniform conductivity profile and allows free charge carriers induced by the electric field [20]. Also it is possible to model a fluid as a perfect conductor in high conductivity limit of the leaky dielectric model [21]. Unlike the leaky dielectric fluids, in perfectly dielectric fluids there are no free charges and electric field occurs due to polarization [34, 35].

The EHD instability between two leaky dielectric, immiscible fluids is examined in many works [21, 29, 31–33, 46–56] and they are summarized not here but in Sections 2.3 and 2.4. In some of these works two perfect fluids are also considered. In some recent works, the focus is only on the interface between two perfect dielectrics [57–59]. Kochurin and Zubarev [57] inspect the dynamics of the interface where an electric field vertical to the initial position of the interface, and gravitational field act on the system. In [58] a configuration, in which the upper electrode is a patterned mask and the lower electrode is flat, is investigated using two perfect dielectric fluids. They form a two-dimensional computational model and analyse the fully nonlinear equations. Kourmatzis and Shrimpton [59] employ a fully nonlinear analysis to examine the morphology of the resulting steady-state interface shapes in the presence of a base Couette flow. It is shown that there are three different regimes, in which single or double convection cells are observed, or a roll structure occurs without the convection cells, or neither of these shapes are observed. Herminghaus [60] conducts a linear stability analysis for the interface between a perfect conductor and a leaky dielectric fluid and gives the wavenumber of the fastest growing mode in terms of the strength of the electric field and dispersive forces. Tseluiko and Papageorgiou [61] study the interface between two perfectly conductive fluids where the upper fluid is infinitely thick and show that even though the interface does not reach the wall in finite time it asymptotically reaches at

infinite time. In another work of the same group [62], the lower electrode is taken as an inclined, corrugated wall. The lower fluid has finite thickness and is either a perfect conductor or a perfect dielectric, whereas the upper fluid is an infinitely thick perfect conductor. It is shown that the behavior of the perfect dielectric film is quantitatively different for permittivity ratios larger than 1 and smaller than 1.

2.3. Direction of the Electric Field

In this section the direction of the applied electric field and the type of the current are examined. The electric field is applied either normal [21,29,31,38,46,48,49,51,63–67] or parallel (tangential) [3, 32, 47, 55, 67] to the initial position of the interface. In most configurations a direct current (DC) electric field is used [3, 21, 29, 31–33, 38, 46, 47, 63, 64, 66, 67]; however, alternating current electric field is also employed in few works [48, 49, 51, 65, 68]. The works, where the electric field is applied normal to the interface via a direct current is presented in Section 2.4.

The linear stability of the interface between a viscous leaky dielectric fluid and a surrounding hydrodynamically passive leaky dielectric fluid is inspected in the presence of a tangential, DC electric field for the charge relaxation times that are much smaller than the hydrodynamic time scale at zero Reynolds number limit in [47]. The regions, in which the interface is unstable are given in terms of the electrical conductivity and permittivity ratios of the fluids. Uguz *et al.* [32] and, Uguz and Aubry [33] investigate the linear stability of two leaky dielectric fluids subjected to a base pressure-driven flow in the presence of a parallel DC electric field in a micro channel. These two works are given in more detail in Section 2.4. Nurocak and Uguz [67] use the leaky dielectric model to inspect the EHD instability between a non-Newtonian and a passive fluid in the presence of an electric field either normal or parallel to the interface.

In few works, physical systems including alternating current (AC) electric fields are examined [48, 49, 65]. Roberts and Kumar [48] employ AC field to destabilize the interface between a polymer and air. The fluids are assumed to be both perfectly or both leaky dielectric. The linear stability analysis reveals that the charge accumulation

at the interface is reduced in high frequencies. A similar system, in which three layers are present, two polymer layers and air, is studied in [65]. The addition of the second polymer layer results in increased complexity in the steady-state interface position profiles. Also, the nonlinear analysis shows that the shapes are drastically different for the leaky dielectric and the perfectly dielectric fluids. Gambhire and Thaokar [49] carry out a linear stability analysis for the interface of two immiscible fluids in the presence of an AC electric field. The fluids are assumed to be either perfect or leaky dielectrics. It is shown that in the high frequency limit, the observations for the leaky and perfect dielectrics are similar, whereas when frequency goes asymptotically to zero, the behavior of the leaky dielectric fluids under an AC field are similar to that of the leaky dielectric fluids under a DC field.

2.4. Mathematical Analysis Methods

Three types of stability analysis giving different informations for the system are present in the literature. The most commonly used method is the linear stability analysis, which gives information about the critical or the neutral point of the instability and shows whether an infinitesimally disturbance on the system dies out or grows. It is not possible to observe the behavior of the interface after it is deflected by using the linear stability analysis. By carrying out a weakly nonlinear stability analysis, the type of the bifurcations is determined [21]. Finally, the fully nonlinear stability analysis gives the time evolution of the interface, e.g. whether it touches a channel wall or reaches a steady-state far from the walls. Unless otherwise mentioned, all works in this section carries out a linear stability analysis.

Shankar and Sharma [46] investigate the stability between two immiscible leaky dielectric fluids and show the effects of the conductivity, dielectric constant, thickness and viscosity ratios on the fastest growing mode and the growth rate of the most unstable mode. Ozen *et al.*determine that the electric field applied to the interface between two leaky dielectric fluids is either stabilizing or destabilizing depending on the physical properties [31]. Then, it is shown that the electric field is always destabilizing for the interface between two perfect dielectrics, whereas it may destabilize or stabilize

the interface in the case of two leaky dielectric fluids depending on the permittivity and conductivity ratios of the fluids [38]. Uguz *et al.* [32] reveals that the linear stability analysis for the interface between two leaky dielectric fluids simplifies significantly for fast electric charge relaxation times. This simplification enables the analytical solution of the linear equations and the regions where a normal and/or a parallel electric field destabilize the interface is given based on the conductivity and the permittivity ratios. It is also shown that the presence of a base pressure-driven flow does not affect the linear stability point. Uguz and Aubry [33], verify the findings of [32] and determine the growth rates and neutral stability curves in the zero Reynolds number limit.

Craster and Matar [29] consider two leaky dielectric fluids in a channel. The fluids are initially stationary and a normal electric field is applied to disturb the interface between them. The nonlinear evolution equations for the interface position and the surface charge density are derived and a parametric study is done. Thaokar and Kumaran [21] examined the interface between either two perfectly dielectric or two leaky dielectric fluids in the presence of a base flow. The base flow is a linear shear flow, which occurs due to the motion of the channel walls. It is shown that the voltage, at which the interface becomes unstable is higher for a perfectly dielectric system compared to a leaky dielectric one, via the linear stability analysis. It is also shown in the presence of the base shear flow, the interface does not reach the walls via lubrication theory. Mahlmann and Papageorgiou [50] solve nonlinear equations in the presence of a base Couette flow and show that drop-like regions near the channel walls emerge as growth rate is increased. Narayanan [69] studies a configuration similar to the physical system of this work. The linear and fully nonlinear analysis are done for two immiscible leaky dielectric fluids, one of which (oil phase) is sandwiched by the other fluid (aqueous phase). The main difference with this work is that [69] has two interfaces. Also a case, in which a base pressure-driven flow is present is studied and it is claimed that the long waves are stabilized by an increase in the pressure gradient, whereas the short waves are destabilized.

Some of the works, which are slightly less similar to ours are given in chronological order. In [66] a similar configuration to [67] is investigated using only a normal,

DC electric field. The linear stability of the interface between a Newtonian and a non-Newtonian fluid is examined. In [52], both linear and nonlinear analysis are done to observe the shape of the steady-state interface position in the presence of either homogeneous or heterogeneous charge distribution at the interface and develop some analytical expressions to estimate these shapes for both perfect and leaky dielectric fluids. Wray *et al.* [70] study a cylindrical configuration in which a leaky dielectric fluid flows in the direction of gravity and is surrounded by a passive fluid. The fluids are between two concentric cylindrical electrodes. Their linear stability analysis reveals that as the strength of the electric field increases the non-axisymmetric modes become more dominant. Ramkrishnan and Kumar [53] inspect the behavior of the interface between a liquid and air. Both leaky and perfect dielectric fluids are considered, and the lower electrode has either a sinusoidal or a trapezoidal cavity, whereas the upper one is flat. The study shows that there is qualitative agreement between the theoretical results and flow visualization experiments. In [54] an electric field and a temperature gradient act on a two layer system simultaneously. It is concluded that the effect of the temperature gradient is dominant for the perfectly dielectric fluids, whereas the leaky dielectric fluids affected by both the temperature gradient and the electric fields. Thaokar [71] investigates the EHD instability at the interface between a Newtonian fluid and a viscoelastic solid in the presence of an oscillatory flow. This work involves both theoretical and experimental parts. It is shown that the EHD instability is destabilized by the oscillatory flow and the applied electric field destabilizes the shear induced instability, which emerges due to the oscillatory flow.

3. PHYSICAL SYSTEM AND MATHEMATICAL MODEL

The physical system is composed of two immiscible, Newtonian and leaky dielectric fluids. The fluids are subjected to a pressure-driven flow in a micro channel and allowed to have different physical properties, viscosity μ, density ρ, electrical conductivity σ, and electrical permittivity $\varepsilon_0\varepsilon$, where ε_0 is the vacuum permittivity. The physical system is depicted in Fig. 3.1, where superscript $\star$ is used to distinguish the upper fluid from the lower one. The lower wall is at $z{=}{-}d$, the upper wall is at $z{=}d^\star$, $z{=}0$ is the position of the flat interface and $z{=}Z(x,t)$ is the interface position. Due the small dimensions of a micro channel, Reynolds number is also small; hence the flow is laminar and the interface is flat at the base state.

It is possible to disturb the flat interface at $z{=}0$ by applying an electric field to the system and at some critical voltage the interface may become unstable [32]. In this work, the direction of the electric field is normal to the flat interface. Since the wavelengths of the disturbances that are applied to the flat interface are much larger than their amplitudes, long wave analysis can be employed and the nonlinear evolutions of the interface position and the surface charge density are studied. In this work, surface coupled model is used. Therefore, there are no electrical terms in the governing equations and they appear only at the interface conditions [19]. The derivation of the electrohydrodynamics equations will not be given here but the details can be found in [72].

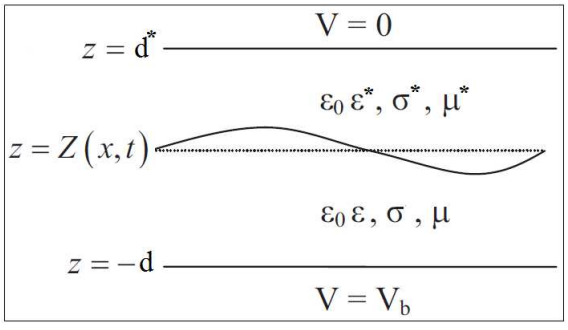

Figure 3.1. Physical system.

The nonlinear governing equations for the electrohydrodynamics are the Navier-Stokes, the continuity and the Laplace equations, and are given as

$$\rho\frac{\partial \underline{v}}{\partial t} + \rho\underline{v}\cdot\nabla\underline{v} = -\nabla p + \mu\nabla^2\underline{v} \tag{3.1}$$

$$\nabla\cdot\underline{v} = 0 \tag{3.2}$$

and

$$\nabla^2 V = 0 \tag{3.3}$$

respectively. Here, $\underline{v}$, p and V are the velocity, pressure and voltage fields, respectively. Corresponding governing equations are valid for the starred ($\star$) fluid as well and are not repeated here. The boundary conditions are given as

$$\underline{v} = \underline{0} \quad \text{at} \quad z = -d, \qquad V = V_b \quad \text{at} \quad z = -d \tag{3.4}$$

and

$$\underline{v}^\star = \underline{0} \quad \text{at} \quad z = d^\star, \qquad V^\star = 0 \quad \text{at} \quad z = d^\star \tag{3.5}$$

The kinematic condition, the no-slip condition, the tangential and the normal components of the stress balances at the interface are given as

$$\underline{v}\cdot\underline{n} = \underline{u}\cdot\underline{n} = \underline{v}^\star\cdot\underline{n} \tag{3.6}$$

$$\underline{v}\cdot\underline{t} = \underline{v}^\star\cdot\underline{t} \tag{3.7}$$

$$\left(\underline{\underline{T}}^{\star} \cdot \underline{n}\right) \cdot \underline{n} - \left(\underline{\underline{T}} \cdot \underline{n}\right) \cdot \underline{n} + \gamma 2H = 0 \tag{3.8}$$

and

$$\left(\underline{\underline{T}}^{\star} \cdot \underline{n}\right) \cdot \underline{t} = \left(\underline{\underline{T}} \cdot \underline{n}\right) \cdot \underline{t} \tag{3.9}$$

respectively. Here, $\underline{\underline{T}}$ is the total stress tensor, γ is interfacial tension. Also, $\underline{u}$ is the velocity of the interface, $2H$ is the twice of the mean curvature, and $\underline{n}$ and $\underline{t}$ are the normal and tangent vectors given as

$$\underline{u} = Z_t \underline{k} \tag{3.10}$$

$$2H = \frac{Z_{xx}}{(1 + Z_x^2)^{\frac{3}{2}}} \tag{3.11}$$

$$\underline{t} = \frac{\underline{i} + Z_x \underline{k}}{(1 + Z_x^2)^{\frac{1}{2}}} \tag{3.12}$$

and

$$\underline{n} = \frac{-Z_x \underline{i} + \underline{k}}{(1 + Z_x^2)^{\frac{1}{2}}} \tag{3.13}$$

respectively [73]. Here Z_x and Z_t are $\frac{\partial Z}{\partial x}$ and $\frac{\partial Z}{\partial t}$, respectively. The total stress tensor is assumed to be composed of two separate parts as

$$\underline{\underline{T}} = \underline{\underline{T}}^F + \underline{\underline{T}}^E \tag{3.14}$$

where $\underline{\underline{T}}^F$ and $\underline{\underline{T}}^E$ are the fluid and the electric stresses and defined as

$$\underline{\underline{T}}^F = -p\underline{\underline{I}} + \mu \left(\nabla \underline{v} + (\nabla \underline{v})^T\right) \tag{3.15}$$

and

$$\underline{\underline{T}}^{E} = \varepsilon_0 \varepsilon \left[\underline{E}\underline{E} - \frac{1}{2} \left(\underline{E} \cdot \underline{E} \right) \underline{\underline{I}} \right] \tag{3.16}$$

respectively. Here, $\underline{\underline{I}}$ is the identity tensor and $\underline{E}$ is the electric field defined as

$$\underline{E} = -\nabla V \tag{3.17}$$

Other equations that should be satisfied at the interface are the continuity of the electric field, the Gauss's law and the conservation of charge and they are given by

$$\underline{E} \cdot \underline{t} = \underline{E}^{\star} \cdot \underline{t} \tag{3.18}$$

$$q = \varepsilon_0 \varepsilon^{\star} \underline{E}^{\star} \cdot \underline{n} - \varepsilon_0 \varepsilon \underline{E} \cdot \underline{n} \tag{3.19}$$

$$q_t - \underline{u} \cdot \nabla_s q + \nabla_s \cdot (q \underline{u}_s) + q 2H \underline{u} \cdot \underline{n} = \sigma \underline{n} \cdot \underline{E} - \sigma^{\star} \underline{n} \cdot \underline{E}^{\star} \tag{3.20}$$

respectively, where q is the surface charge density. In Section 3.1, first, the governing equations and the boundary and the interface conditions will be nondimensionalized and then the dominant terms in the equations will be determined based on the lubrication theory.

3.1. Scaling and Dominant Terms

Following characteristic scales are used to nondimensionalize the governing equations and the boundary and the interface conditions:

$$\tilde{x} = \frac{x}{L} \qquad \tilde{z} = \frac{z}{d} \qquad \tilde{Z} = \frac{Z}{d} \qquad \tilde{u} = \frac{u}{U}$$
$$\tilde{w} = \frac{Lw}{dU} \qquad \tilde{t} = \frac{Ut}{L} \qquad \tilde{p} = \frac{d^2 p}{\mu U L} \qquad \tilde{V} = \frac{V}{V_b} \qquad \tilde{q} = \frac{dq}{\varepsilon_0 V_b} \quad (3.21)$$

Here, L and d are the channel length and width of the unstarred fluid; and based on the lubrication theory it is assumed that the width of the channel is much smaller than its length, i.e. $d/L{=}\epsilon$, where $\epsilon << 1$. Also u and w are the x and z components of the velocity, U is the speed of the interface when the interface is flat and V_b is the base state voltage applied at $Z{=}{-}d$. Next, the governing equations are nondimensionalized.

3.1.1. Governing Equations

The nondimensionalized governing equations for the unstarred fluid are found as

$$\epsilon^2 Re(\tilde{u}_{\tilde{t}} + \tilde{u}\tilde{u}_{\tilde{x}} + \tilde{w}\tilde{u}_{\tilde{z}}) = -\tilde{p}_{\tilde{x}} + \epsilon^2 \tilde{u}_{\tilde{x}\tilde{x}} + \tilde{u}_{\tilde{z}\tilde{z}} \quad (3.22)$$

$$\epsilon^4 Re(\tilde{w}_{\tilde{t}} + \tilde{u}\tilde{w}_{\tilde{x}} + \tilde{w}\tilde{w}_{\tilde{z}}) = -\tilde{p}_{\tilde{z}} + \epsilon^4 \tilde{w}_{\tilde{x}\tilde{x}} + \epsilon^2 \tilde{w}_{\tilde{z}\tilde{z}} \quad (3.23)$$

$$\tilde{u}_{\tilde{x}} + \tilde{w}_{\tilde{z}} = 0 \quad (3.24)$$

and

$$\tilde{V}_{\tilde{z}\tilde{z}} + \epsilon^2 \tilde{V}_{\tilde{x}\tilde{x}} = 0 \quad (3.25)$$

where Reynolds number Re is defined as

$$Re = \frac{\rho U L}{\mu} \quad (3.26)$$

The governing equations for the starred fluid is written in dimensionless form as

$$\epsilon^2 Re\frac{\phi}{\lambda}(\tilde{u}^\star_{\tilde{t}} + \tilde{u}^\star\tilde{u}^\star_{\tilde{x}} + \tilde{w}^\star\tilde{u}^\star_{\tilde{z}}) = -\frac{1}{\lambda}\tilde{p}^\star_{\tilde{x}} + \epsilon^2\tilde{u}^\star_{\tilde{x}\tilde{x}} + \tilde{u}^\star_{\tilde{z}\tilde{z}} \tag{3.27}$$

$$\epsilon^4 Re\frac{\phi}{\lambda}(\tilde{w}^\star_{\tilde{t}} + \tilde{u}^\star\tilde{w}^\star_{\tilde{x}} + \tilde{w}^\star\tilde{w}^\star_{\tilde{z}}) = -\frac{1}{\lambda}\tilde{p}^\star_{\tilde{z}} + \epsilon^4\tilde{w}^\star_{\tilde{x}\tilde{x}} + \epsilon^2\tilde{w}^\star_{\tilde{z}\tilde{z}} \tag{3.28}$$

$$\tilde{u}^\star_{\tilde{x}} + \tilde{w}^\star_{\tilde{z}} = 0 \tag{3.29}$$

and

$$\tilde{V}^\star_{\tilde{z}\tilde{z}} + \epsilon^2\tilde{V}^\star_{\tilde{x}\tilde{x}} = 0 \tag{3.30}$$

where ϕ and λ are the density and the viscosity ratios defined as

$$\phi = \frac{\rho^\star}{\rho} \qquad \lambda = \frac{\mu^\star}{\mu} \tag{3.31}$$

3.1.2. Boundary and Interface Conditions

The dimensionless boundary conditions are

$$\tilde{u}(-1) = 0 \qquad \tilde{V}(-1) = 1 \qquad \tilde{u}^\star(\beta) = 0 \qquad \tilde{V}^\star(\beta) = 0 \tag{3.32}$$

where β is the depth ratio defined as

$$\beta = \frac{d^\star}{d} \tag{3.33}$$

The interface conditions, the kinematic condition Equation 3.6, the no-slip condition Equation 3.7, the normal stress balance Equation 3.8, the tangential stress balance

Equation 3.9, the continuity of the electric field Equation 3.18, the Gauss's law Equation 3.19 and the charge conservation Equation 3.20 are given in dimensionless form by

$$\tilde{u}\tilde{Z}_{\tilde{x}} + \tilde{w} = \tilde{Z}_{\tilde{t}} = \tilde{u}^{\star}\tilde{Z}_{\tilde{x}} + \tilde{w}^{\star} \tag{3.34}$$

$$\tilde{u} + \epsilon^2 \tilde{Z}_{\tilde{x}}\tilde{w} = \tilde{u}^{\star} + \epsilon^2 \tilde{Z}_{\tilde{x}}\tilde{w}^{\star} \tag{3.35}$$

$$\begin{aligned}(\tilde{p} - \tilde{p}^{\star}) + \frac{\lambda\epsilon^2}{1+\epsilon^2\tilde{Z}_{\tilde{x}}^2}\left[2\tilde{u}_{\tilde{x}}^{\star}\left(\epsilon^2\tilde{Z}_{\tilde{x}}^2 - 1\right) - 2\tilde{Z}_{\tilde{x}}\left(\tilde{u}_{\tilde{z}}^{\star} + \epsilon^2\tilde{w}_{\tilde{x}}^{\star}\right)\right] \\ + Eb\frac{\varepsilon^{\star}}{1+\epsilon^2\tilde{Z}_{\tilde{x}}^2}\left[\frac{1}{2}\left(1-\epsilon^2\tilde{Z}_{\tilde{x}}^2\right)\left(\tilde{V}_{\tilde{z}}^{\star 2} - \epsilon^2\tilde{V}_{\tilde{x}}^{\star 2}\right) - \epsilon^2\tilde{Z}_{\tilde{x}}\tilde{V}_{\tilde{x}}^{\star}\tilde{V}_{\tilde{z}}^{\star}\right] \\ - \frac{\epsilon^2}{1+\epsilon^2\tilde{Z}_{\tilde{x}}^2}\left[2\tilde{u}_{\tilde{x}}\left(\epsilon^2\tilde{Z}_{\tilde{x}}^2 - 1\right) - 2\tilde{Z}_{\tilde{x}}\left(\tilde{u}_{\tilde{z}} + \epsilon^2\tilde{w}_{\tilde{x}}\right)\right] \\ - Eb\frac{\varepsilon}{1+\epsilon^2\tilde{Z}_{\tilde{x}}^2}\left[\frac{1}{2}\left(1-\epsilon^2\tilde{Z}_{\tilde{x}}^2\right)\left(\tilde{V}_{\tilde{z}}^{2} - \epsilon^2\tilde{V}_{\tilde{x}}^{2}\right) - \epsilon^2\tilde{Z}_{\tilde{x}}\tilde{V}_{\tilde{x}}\tilde{V}_{\tilde{z}}\right] + \frac{\epsilon^3}{Ca}\frac{\tilde{Z}_{\tilde{x}\tilde{x}}}{\left(1+\epsilon^2\tilde{Z}_{\tilde{x}}^2\right)^{\frac{3}{2}}} = 0\end{aligned} \tag{3.36}$$

$$\begin{aligned}\left[-4\epsilon^2\tilde{Z}_{\tilde{x}}\tilde{u}_{\tilde{x}} + \left(\epsilon^2\tilde{w}_{\tilde{x}} + \tilde{u}_{\tilde{z}}\right)\left(1-\epsilon^2\tilde{Z}_{\tilde{x}}^2\right)\right] - \lambda\left[-4\epsilon^2\tilde{Z}_{\tilde{x}}\tilde{u}_{\tilde{x}}^{\star} + \left(\epsilon^2\tilde{w}_{\tilde{x}}^{\star} + \tilde{u}_{\tilde{z}}^{\star}\right)\left(1-\epsilon^2\tilde{Z}_{\tilde{x}}^2\right)\right] \\ Eb\,\tilde{q}\left(1+\epsilon^2\tilde{Z}_{\tilde{x}}^2\right)^{\frac{1}{2}}\left(\tilde{V}_{\tilde{x}} + \tilde{Z}_{\tilde{x}}\tilde{V}_{\tilde{z}}\right) = 0\end{aligned} \tag{3.37}$$

$$\tilde{V}_{\tilde{x}} + \tilde{V}_{\tilde{z}}\tilde{Z}_{\tilde{x}} = \tilde{V}_{\tilde{x}}^{\star} + \tilde{V}_{\tilde{z}}^{\star}\tilde{Z}_{\tilde{x}} \tag{3.38}$$

$$\tilde{q} = \frac{1}{(1+\epsilon^2 Z_x^2)^{\frac{1}{2}}}\left(\varepsilon^{\star}(\epsilon^2\tilde{Z}_{\tilde{x}}\tilde{V}_{\tilde{x}}^{\star} - \tilde{V}_{\tilde{z}}^{\star}) - \varepsilon(\epsilon^2\tilde{Z}_{\tilde{x}}\tilde{V}_{\tilde{x}} - \tilde{V}_{\tilde{z}})\right) \tag{3.39}$$

and

$$\tilde{q}_{\tilde{t}} - \epsilon^2 \frac{\tilde{Z}_{\tilde{t}}\tilde{Z}_{\tilde{x}}}{(1+\epsilon^2\tilde{Z}_{\tilde{x}}^2)}\tilde{q}_{\tilde{x}} + \frac{1}{(1+\epsilon^2\tilde{Z}_{\tilde{x}}^2)^{\frac{1}{2}}}\left(\frac{\tilde{u}+\epsilon^2\tilde{w}\tilde{Z}_{\tilde{x}}}{(1+\epsilon^2\tilde{Z}_{\tilde{x}}^2)^2}\tilde{q}\right)_{\tilde{x}} + \epsilon^2\tilde{Z}_{\tilde{x}\tilde{x}}\frac{\tilde{w}-\tilde{u}\tilde{Z}_{\tilde{x}}}{(1+\epsilon^2\tilde{Z}_{\tilde{x}}^2)^2}\tilde{q}$$
$$= S\frac{1}{(1+\epsilon^2\tilde{Z}_{\tilde{x}}^2)^{\frac{1}{2}}}\left[\left(\epsilon^2\tilde{Z}_{\tilde{x}}\tilde{V}_{\tilde{x}} - \tilde{V}_{\tilde{z}}\right) - \alpha\left(\epsilon^2\tilde{Z}_{\tilde{x}}\tilde{V}^{\star}_{\tilde{x}} - \tilde{V}^{\star}_{\tilde{z}}\right)\right] \quad (3.40)$$

where S is a dimensionless parameter, which shows the ratio of the fluid to electric time scale, α is the conductivity ratio, Ca is the capillary number and Eb is the electric number defined as

$$S = \frac{L\sigma}{\varepsilon_0 U} \qquad \alpha = \frac{\sigma^{\star}}{\sigma} \qquad Ca = \frac{\mu U}{\gamma} \qquad Eb = \frac{\varepsilon_0 \Delta V^2}{\mu U L} \quad (3.41)$$

respectively.

3.2. Base State Profiles

To obtain the base state equations, the dominant terms of the governing equations and the interface conditions are determined. From now on, tildes will be dropped and subscript 0 will be used to denote the base state variables. Since $\epsilon << 1$, the dominant terms for the governing equations for the unstarred fluid Equations 3.22 to 3.25 can be written as

$$0 = -p_{0,x} + u_{0,zz} \quad (3.42)$$

$$0 = -p_{0,z} \quad (3.43)$$

$$V_{0,zz} = 0 \quad (3.44)$$

and

$$u_{0,x} + w_{0,z} = 0 \tag{3.45}$$

The dominant terms of the governing equations for the starred fluid Equations 3.27 to 3.30 are

$$0 = -\frac{1}{\lambda} p^{\star}_{0,x} + u^{\star}_{0,zz} \tag{3.46}$$

$$0 = -p^{\star}_{0,z} \tag{3.47}$$

$$V^{\star}_{0,zz} = 0 \tag{3.48}$$

and

$$u^{\star}_{0,x} + w^{\star}_{0,z} = 0 \tag{3.49}$$

Again by recalling that $\epsilon << 1$, the dominant terms for the interface equations Equations 3.33 to 3.40 are given as

$$w_0 - u_0 Z_{0,x} = Z_{0,t} = w^{\star}_0 - u^{\star}_0 Z_{0,x} \tag{3.50}$$

$$u_0 = u^{\star}_0 \tag{3.51}$$

$$p_0 - p^{\star}_0 - \frac{Eb}{2}\left(\varepsilon V^2_{0,z} - \varepsilon^{\star} V^{\star 2}_{0,z}\right) + \frac{\epsilon^3}{Ca} Z_{0,xx} = 0 \tag{3.52}$$

$$u_{0,z} - \lambda u^{\star}_{0,z} = -Eb\, q_0 \left(V_{0,x} + Z_{0,x} V_{0,z}\right) \tag{3.53}$$

$$V_{0,x} + Z_{0,x} V_{0,z} = V^{\star}_{0,x} + Z_{0,x} V^{\star}_{0,z} \tag{3.54}$$

$$q_0 = \varepsilon V_{0,z} - \varepsilon^{\star} V^{\star}_{0,z} \tag{3.55}$$

and

$$q_{0,t} + \left(u_0 q_0\right)_x = S\left(\alpha V^{\star}_{0,z} - V_{0,z}\right) \tag{3.56}$$

The dominant terms for the dimensionless boundary conditions given in Equation 3.32 are written as

$$u_0(-1) = 0, \qquad V_0(-1) = 1, \qquad u^{\star}_0(\beta) = 0, \qquad V^{\star}_0(\beta) = 0 \tag{3.57}$$

Next step before the perturbation is to solve the base state equations, where the interface is flat and Z=0. The governing equations, i.e. Equations 3.42 to 3.49 and two of the interface condition Equation 3.51 and Equation 3.55 remain the same. Therefore they are not repeated here and only the other interface conditions will be given. Since Z=0 and constant with respect to time and position, Equation 3.50 yields

$$w_0 = 0 = w^{\star}_0 \tag{3.58}$$

At the flat interface, the normal stress balance Equation 3.52 reduces to

$$p_0 - p^{\star}_0 - \frac{Eb}{2}\left(\varepsilon V^2_{0,z} - \varepsilon^{\star} V^{\star 2}_{0,z}\right) = 0 \tag{3.59}$$

and the tangential component of the stress balance Equation 3.53 yields

$$u_{0,z} = \lambda u^{\star}_{0,z} \tag{3.60}$$

since the base state voltage profiles are not x-dependent and Z=0. At the flat interface, Equation 3.54 becomes

$$V_{0,x} = V^{\star}_{0,x} \tag{3.61}$$

The voltage profiles when the interface is flat, are not x-dependent and the derivatives of the voltages of the starred and unstarred fluids with respect to x are zero. Therefore, the continuity of the electric field is automatically satisfied. However, by integrating along one wavelength with respect to x, it can be seen that the continuity of the electric field should also satisfy

$$V_0 = V^{\star}_0 \tag{3.62}$$

The base state flow is assumed to be fully developed and the base state charge density is constant. Therefore, the velocity profiles of both fluids are not x-dependent and the base state charge density does not depend on time or position. Then, Equation 3.56 reduces to

$$V_{0,z} = \alpha V^{\star}_{0,z} \tag{3.63}$$

Now, the governing equations Equations 3.42 to 3.49 will be solved. The z-components of the Navier-Stokes equations for both fluids, Equation 3.43 and Equation 3.47, indicate that p_0 and $p^{\star}_0$ are not z-dependent. Therefore, by integrating Equation 3.42 twice with respect to z, the base state velocity profile of the unstarred fluid is found as

$$u_0 = \frac{1}{2} p_{0,x} z^2 + a_0 z + b_0 \tag{3.64}$$

and similarly, by integrating Equation 3.46, the base state velocity profile for the starred fluid is written as

$$u_0^\star = \frac{1}{2\lambda} p_{0,x}^\star z^2 + a_0^\star z + b_0^\star \tag{3.65}$$

where a_0, $a_0^\star$, b_0 and $b_0^\star$ are the integration constants. The velocity profiles have a total of six unknowns and to determine the unknowns, two boundary conditions at the walls, the no-slip condition, the tangential stress balance, the derivative of the normal stress balance with respect to x and the definition of the characteristic velocity scale will be used. The boundary conditions at the walls are given by Equation 3.32. The no-slip condition indicates that the velocities of the fluids are equal at z=0. Also, since the velocity scale is the speed at the interface when it is flat, i.e. Z=0

$$u_0(0) = 1 = u_0^\star(0) \tag{3.66}$$

The base state voltage profiles are not x-dependent. Therefore, the derivative of the normal stress balance with respect to x yields

$$p_{0,x} = p_{0,x}^\star \tag{3.67}$$

By using the boundary conditions and Equation 3.60 and Equation 3.67, the velocity profiles for unstarred and starred fluids are found as

$$u_0 = -\frac{\lambda + \beta}{\beta\,(\beta + 1)} z^2 - \frac{\lambda - \beta^2}{\beta\,(\beta + 1)} z + 1 \tag{3.68}$$

and

$$u_0^\star = -\frac{1}{\lambda}\frac{\lambda + \beta}{\beta\,(\beta + 1)} z^2 - \frac{1}{\lambda}\frac{\lambda - \beta^2}{\beta\,(\beta + 1)} z + 1 \tag{3.69}$$

respectively. By integrating Equation 3.45 and Equation 3.49 twice with respect to z, the linear voltage profiles are found as

$$V_0 = c_0 z + g_0 \tag{3.70}$$

and

$$V_0^\star = c_0^\star z + g_0^\star \tag{3.71}$$

Using the boundary conditions Equation 3.32, and Equation 3.62 and Equation 3.63 the scaled base state voltage profiles are found as

$$V_0 = -\frac{\alpha}{\alpha+\beta} z + \frac{\beta}{\alpha+\beta} \tag{3.72}$$

and

$$V_0^\star = -\frac{1}{\alpha+\beta} z + \frac{\beta}{\alpha+\beta} \tag{3.73}$$

By substituting the voltage profiles in Equation 3.55, the surface charge density at the flat interface is determined as

$$q_0 = \frac{\varepsilon^\star - \alpha\varepsilon}{\alpha+\beta} \tag{3.74}$$

Now, all base state variables are known. In Section 3.3, the equations will be perturbed and the nonlinear evolution of the interface and the surface charge density will be investigated.

3.3. Derivation of the Perturbed Equations

In this section, the interface is perturbed with a small disturbance and Z is not zero anymore. Perturbing the governing equations, i.e. Equations 3.42 to 3.49 gives

$$p_{0,x} + \hat{p}_x = u_{0,zz} + \hat{u}_{zz} \tag{3.75}$$

$$p_{0,z} + \hat{p}_z = 0 \tag{3.76}$$

$$V_{0,zz} + \hat{V}_{zz} = 0 \tag{3.77}$$

$$u_{0,x} + \hat{u}_x + w_{0,z} + \hat{w}_z = 0 \tag{3.78}$$

$$\frac{1}{\lambda}\left(p^{\star}_{0,x} + \hat{p}^{\star}_x\right) = u^{\star}_{0,zz} + \hat{u}^{\star}_{zz} \tag{3.79}$$

$$p^{\star}_{0,z} + \hat{p}^{\star}_z = 0 \tag{3.80}$$

$$V^{\star}_{0,zz} + \hat{V}^{\star}_{zz} = 0 \tag{3.81}$$

and

$$u^{\star}_{0,x} + \hat{u}^{\star}_x + w^{\star}_{0,z} + \hat{w}^{\star}_z = 0 \tag{3.82}$$

where, hats denote the perturbed variables. Since the base state governing equations are valid at any point regardless of the position of the interface, subtracting Equations

3.42 to 3.49 from Equations 3.75 to 3.82 yields

$$\hat{p}_x = \hat{u}_{zz} \tag{3.83}$$

$$\hat{p}_z = 0 \tag{3.84}$$

$$\hat{V}_{zz} = 0 \tag{3.85}$$

$$\hat{u}_x + \hat{w}_z = 0 \tag{3.86}$$

$$\frac{1}{\lambda}\hat{p}^\star_x = \hat{u}^\star_{zz} \tag{3.87}$$

$$\hat{p}^\star_z = 0 \tag{3.88}$$

$$\hat{V}^\star_{zz} = 0 \tag{3.89}$$

and

$$\hat{u}^\star_x + \hat{w}^\star_z = 0 \tag{3.90}$$

The perturbed boundary conditions can be written as

$$\hat{u}^\star(\beta) = 0 \qquad \hat{w}^\star(\beta) = 0 \qquad \hat{V}^\star(\beta) = 0 \tag{3.91}$$

and

$$\hat{u}(-1) = 0 \qquad \hat{w}(-1) = 0 \qquad \hat{V}(-1) = 0 \tag{3.92}$$

The interface conditions at the perturbed interface, i.e. at $Z{=}Z(x,t)$, are written starting with the kinematic condition Equation 3.50, i.e.

$$(w_0 + \hat{w}) - (u_0 + \hat{u})\,\hat{Z}_x = \hat{Z}_t = (w_0^\star + \hat{w}^\star) - (u_0^\star + \hat{u}^\star)\,\hat{Z}_x \tag{3.93}$$

and it simplifies into

$$\hat{w} - (u_0 + \hat{u})\,\hat{Z}_x = \hat{Z}_t = \hat{w}^\star - (u_0^\star + \hat{u}^\star)\,\hat{Z}_x \tag{3.94}$$

since the z-components of the base state velocities are zero. The no-slip condition Equation 3.51 yields

$$u_0 + \hat{u} = u_0^\star + \hat{u}^\star \tag{3.95}$$

Here, it is important to notice that the base state velocities of the starred and unstarred fluids are equal to each other only at the flat interface. Therefore, Equation 3.95 can not be simplified further when the interface is perturbed. The normal stress balance Equation 3.52 is perturbed as

$$(p_0 + \hat{p}) - (p_0^\star + \hat{p}^\star) - \frac{1}{2}Eb\left[\varepsilon\left(V_{0,z} + \hat{V}_z\right)^2 - \varepsilon^\star\left(V_{0,z}^\star + \hat{V}_z^\star\right)^2\right] + \frac{\epsilon^3}{Ca}\hat{Z}_{xx} = 0 \tag{3.96}$$

By using the base state normal stress balance Equation 3.59 and letting $\epsilon^3 = Ca$, the perturbed normal stress balance reduces to

$$(\hat{p} - \hat{p}^\star) - \frac{1}{2}Eb\left[\varepsilon\left(\hat{V}_z^2 + 2V_{0,z}\hat{V}_z\right) - \varepsilon^\star\left(\hat{V}_z^{\star 2} + 2V_{0,z}^\star\hat{V}_z^\star\right)\right] + \hat{Z}_{xx} = 0 \tag{3.97}$$

Note that the capillarity should be kept in the equation as it is responsible for the stabilization of the interface. By letting $\epsilon^3 = Ca$ implicitly non viscous fluids are considered for this analysis. The tangential component of the perturbed stress balance is

$$(u_{0,z} + \hat{u}_z) - \lambda \left(u^\star_{0,z} + \hat{u}^\star_z\right) = Eb\,(q_0 + \hat{q}) \left[\left(V_{0,x} + \hat{V}_x\right) + \hat{Z}_x \left(V_{0,z} + \hat{V}_z\right)\right] \tag{3.98}$$

Although, the base state velocities of the fluids at the interface are not equal when the interface is disturbed, by analysing the base state velocity profiles, it can be seen that

$$u_{0,z} = \lambda u^\star_{0,z} \tag{3.99}$$

Therefore, also by noticing that the base state voltage is not a function of x, the tangential stress balance is simplified to

$$\hat{u}_z - \lambda \hat{u}^\star_z = Eb\,(q_0 + \hat{q}) \left[\hat{V}_x + \hat{Z}_x \left(V_{0,z} + \hat{V}_z\right)\right] \tag{3.100}$$

The continuity of the electric field Equation 3.54 becomes

$$\hat{V}_x + \left(V_{0,z} + \hat{V}_z\right) \hat{Z}_x = \hat{V}^\star_x + \left(V^\star_{0,z} + \hat{V}^\star_z\right) \hat{Z}_x \tag{3.101}$$

Since all terms in Equation 3.55 are constant, the equation is also valid when the interface is disturbed and the perturbed Gauss's law can be written as

$$\hat{q} = \varepsilon \hat{V}_z - \varepsilon^\star \hat{V}^\star_z \tag{3.102}$$

The charge conservation Equation 3.56 is perturbed as

$$q_{0,t} + \hat{q}_t + \left[(u_0 + \hat{u})\,(q_0 + \hat{q})\right]_x = S \left[\alpha \left(V^\star_{0,z} + \hat{V}^\star_z\right) - \left(V_{0,z} + \hat{V}_z\right)\right] \tag{3.103}$$

By using Equation 3.63 and noticing that the base state surface charge density is not time dependent, Equation 3.103 reduces to

$$\hat{q}_t + \left[\left(u_0 + \hat{u}\right)\left(q_0 + \hat{q}\right)\right]_x = S\left(\alpha \hat{V}_z^\star - \hat{V}_z\right) \tag{3.104}$$

3.4. Solutions of the Perturbed Equations

This section starts with the solutions of the perturbed governing equations and the aim is to reduce the equation system to two unknowns, namely the interface position Z and the surface charge density q. Hereafter, Z is used instead of $\hat{Z}$, since Z_0=0. Equations 3.84 and 3.88 indicate that the perturbed pressures of both unstarred and starred fluids are not functions of the coordinate z, but that does not mean that they are not functions of the interface position Z. By using Equation 3.83 and Equation 3.87 x-components of the velocities are found as

$$\hat{u} = \frac{1}{2}\hat{p}_x z^2 + az + b \tag{3.105}$$

and

$$\hat{u}^\star = \frac{1}{2\lambda}\hat{p}_x^\star z^2 + a^\star z + b^\star \tag{3.106}$$

where a, $a^\star$, b and $b^\star$ are the integration constants. Notice that the integral constants may depend on the coordinate x. Applying the boundary conditions given by Equation 3.91 and Equation 3.92, the velocity profiles are written as

$$\hat{u} = \frac{1}{2}\hat{p}_x\left(z^2 - 1\right) + a\left(z + 1\right) \tag{3.107}$$

and

$$\hat{u}^\star = \frac{1}{2}\hat{p}_x^\star\left(z^2 - \beta^2\right) + a^\star\left(z - \beta\right) \tag{3.108}$$

The continuity equations for the unstarred and the starred fluids, Equation 3.86 and Equation 3.90 give the z-components of the velocities as

$$\hat{w} = -\frac{1}{2}\hat{p}_{xx}\left(\frac{z^3}{3} - z\right) - a_x\left(\frac{z^2}{2} + z\right) + e \tag{3.109}$$

and

$$\hat{w}^\star = -\frac{1}{2\lambda}\hat{p}^\star_{xx}\left(\frac{z^3}{3} - \beta^2 z\right) - a^\star_x\left(\frac{z^2}{2} - \beta z\right) + e^\star \tag{3.110}$$

respectively. Here, e and $e^\star$ are the integration constants and determined using the boundary conditions given in Section 3.3. By substituting the integral constants in Equation 3.107 and Equation 3.108 the z-components of the velocities are determined as

$$\hat{w} = -\frac{1}{6}\hat{p}_{xx}\left(z^3 - 3z - 2\right) - \frac{a_x}{2}\left(z^2 + 2z + 1\right) \tag{3.111}$$

and

$$\hat{w}^\star = -\frac{1}{6\lambda}\hat{p}^\star_{xx}\left(z^3 - 3\beta^2 z + 2\beta^3\right) - \frac{a^\star_x}{2}\left(z^2 - 2\beta z + \beta^2\right) \tag{3.112}$$

For the voltage profiles, the Laplace equations Equation 3.85 and Equation 3.89 are used and by applying the boundary conditions given in Section 3.3, the profiles are found as

$$\hat{V} = c\,(z + 1) \tag{3.113}$$

and

$$\hat{V}^\star = c^\star\,(z - \beta) \tag{3.114}$$

Solutions of the perturbed governing equations include eight unknowns, a, $a^\star$, $\hat{p}_x$, $\hat{p}_x^\star$, c, $c^\star$, Z and q, which require eight boundary conditions. First, by using the relations deduced from the continuity of the electric field and the Gauss's law Equation 3.101 and Equation 3.102, respectively, c and $c^\star$ will be determined as functions of Z and q. Then, combining Equation 3.95, Equation 3.100, one of the equalities from Equation 3.94 and the derivative of Equation 3.97 with respect to x, will relate a, $a^\star$, $\hat{p}_x$, $\hat{p}_x^\star$ to the interface position and the surface charge density. By substituting the perturbed voltage profiles, i.e. Equation 3.113 and Equation 3.114 in Equation 3.101 gives

$$c_x\left(Z+1\right)+V_{0,z}Z_x+cZ_x=c_x^\star\left(Z-\beta\right)+V_{0,z}^\star Z_x+c^\star Z_x \tag{3.115}$$

It should be noted that z in the voltage profiles is not the interface position. Therefore, its derivatives with respect to x is zero. First, the x-derivatives of the profiles are taken and then $z=Z$ is substituted in the resulting equations. Rearranging Equation 3.115 gives

$$\left[c\left(Z+1\right)\right]_x-\left(\frac{\alpha}{\alpha+\beta}\right)Z_x=\left[c^\star\left(Z-\beta\right)\right]_x-\left(\frac{1}{\alpha+\beta}\right)Z_x \tag{3.116}$$

and by integrating with respect to x over one wavelength yields

$$c^\star=c\,\frac{Z+1}{Z-\beta}+\frac{1-\alpha}{\alpha+\beta}\,\frac{Z}{Z-\beta} \tag{3.117}$$

Substituting the perturbed voltage profiles in Equation 3.102 gives

$$\hat{q}=\varepsilon c-\varepsilon^\star c^\star \tag{3.118}$$

By combining Equation 3.117 and Equation 3.118, c is found as

$$c=\frac{\hat{q}\left(Z-\beta\right)+\varepsilon^\star\frac{1-\alpha}{\alpha+\beta}Z}{\varepsilon\left(Z-\beta\right)-\varepsilon^\star\left(Z+1\right)} \tag{3.119}$$

Equation 3.117 relates $c^\star$ to c and Equation 3.119 gives c as a function of only the interface position and the surface charge. Therefore, both c and $c^\star$ are known as functions of Z and q only. Substituting the perturbed velocity profiles in Equation 3.95 gives

$$u_0 + \frac{1}{2}\hat{p}_x\left(Z^2-1\right) + a\left(Z+1\right) = u_0^\star + \frac{1}{2}\hat{p}_x^\star\left(Z^2-\beta^2\right) + a^\star\left(Z-\beta\right) \tag{3.120}$$

By inserting the voltage and the velocity profiles, Equation 3.100 can be written as

$$-\hat{p}_x^\star Z - \lambda a^\star + \hat{p}_x Z + a = -Eb\left(\hat{q}+q_0\right)\left[c_x\left(Z+1\right) + \left(c - \frac{\alpha}{\alpha+\beta}\right)Z_x\right] \tag{3.121}$$

and rearranging Equation 3.121 yields

$$a = \lambda a^\star - \left(\hat{p}_x - \hat{p}_x^\star\right)Z - Eb\left(q_0+\hat{q}\right)\left[\left(c - \frac{\alpha}{\alpha+\beta}\right)\left(Z+1\right)\right]_x \tag{3.122}$$

Here, one of the equalities from Equation 3.94 will be used:

$$\hat{w} - \left(u_0+\hat{u}\right)Z_x = \hat{w}^\star - \left(u_0^\star + \hat{u}^\star\right)Z_x \tag{3.123}$$

Inserting the perturbed velocity profiles in Equation 3.123 and rearranging gives

$$\begin{aligned}\left[-\frac{1}{6}\hat{p}_x\left(Z^3-3Z-2\right) - \frac{a}{2}\left(Z+1\right)^2\right]_x - u_0 Z_x \\ = \left[-\frac{1}{6\lambda}\hat{p}_x^\star\left(Z^3-3\beta^2+2\beta^3\right) - \frac{a^\star}{2}\left(Z-\beta\right)^2\right]_x - u_0^\star Z_x\end{aligned} \tag{3.124}$$

Substituting the voltage profiles in Equation 3.97 gives

$$\begin{aligned}\left(\hat{p}-\hat{p}^\star\right) - \frac{1}{2}Eb\left[\varepsilon\left(c^2 + 2\left(-\frac{\alpha}{\alpha+\beta}\right)c\right) - \varepsilon^\star\left(c^{\star 2} + 2\left(-\frac{1}{\alpha+\beta}\right)c^\star\right)\right] \\ + Z_{xx} = 0\end{aligned} \tag{3.125}$$

By rearranging, the derivative of Equation 3.125 is written as

$$\hat{p}_x - \hat{p}_x^\star - \frac{1}{2}Eb\left[\varepsilon\left(\left(c - \frac{\alpha}{\alpha+\beta}\right)^2\right)_x - \varepsilon^\star\left(\left(c^\star - \frac{1}{\alpha+\beta}\right)^2\right)_x\right] + Z_{xxx} = 0 \quad (3.126)$$

Substituting the constant a using Equation 3.122 in Equation 3.120 results in

$$\begin{aligned} u_0 + \frac{1}{2}\hat{p}_x\left(Z^2-1\right) & \\ + \left[\lambda a^\star - \left(\hat{p}_x - \hat{p}_x^\star\right)Z - Eb\left(q_0+\hat{q}\right)\left[\left(c - \frac{\alpha}{\alpha+\beta}\right)(Z+1)\right]_x\right](Z+1) & \\ = u_0^\star + \frac{1}{2}\hat{p}_x^\star\left(Z^2-\beta^2\right) + a^\star\left(Z-\beta\right) & \quad (3.127) \end{aligned}$$

which is rearranged as

$$a^\star N_1 = N_2\hat{p}_x^\star + N_3\hat{p}_x + N_4\left(q_0+\hat{q}\right)(Z+1) + \left(u_0 - u_0^\star\right) \quad (3.128)$$

where

$$N_1 = \left[Z\left(1-\lambda\right) - \left(\lambda+\beta\right)\right] \quad (3.129)$$

$$N_2 = -\frac{1}{2\lambda}\left[Z^2\left(1-2\lambda\right) - \beta^2 - 2\lambda Z\right] \quad (3.130)$$

$$N_3 = -\frac{1}{2}\left(Z+1\right)^2 \quad (3.131)$$

and

$$N_4 = -Eb\left[\left(c - \frac{\alpha}{\alpha+\beta}\right)(Z+1)\right]_x \quad (3.132)$$

Combining Equation 3.122 and Equation 3.128 gives a as

$$a = \hat{p}_x^\star \left[\lambda \frac{N_2}{N_1} + Z\right] + \hat{p}_x \left[\lambda \frac{N_3}{N_1} - Z\right] + (q_0 + \hat{q}) \left[\lambda \frac{N_4}{N_1}(Z+1) + N_4\right] + \frac{\lambda}{N_1}(u_0 - u_0^\star) \quad (3.133)$$

After a and $a^\star$ are found, Equation 3.124 can be rewritten as

$$\hat{p}_x^\star N_5 = -\hat{p}_x N_6 - (q_0 + \hat{q}) N_7 + N_B \quad (3.134)$$

where

$$N_5 = \left[\frac{1}{6\lambda}(Z+2\beta)(Z-\beta)^2 + (Z-\beta)^2 \frac{N_2}{2N_1} - (Z+1)^2 \left(\lambda \frac{N_2}{2N_1} + \frac{Z}{2}\right)\right] \quad (3.135)$$

$$N_6 = \left[-\frac{1}{6}(Z-2)(Z+1)^2 + (Z-\beta)^2 \frac{N_3}{2N_1} - (Z+1)^2 \left(\lambda \frac{N_3}{2N_1} - \frac{Z}{2}\right)\right] \quad (3.136)$$

$$N_7 = \left[-\frac{(Z+1)^2}{2}\left(\lambda \frac{N_4}{N_1}(Z+1) + N_4\right) + \frac{(Z-\beta)^2}{2}\frac{N_4}{N_1}(Z+1)\right] \quad (3.137)$$

and

$$N_B = (u_0 - u_0^\star)\left[Z + \frac{1}{2N_1}\left(\lambda(Z+1)^2 - (Z-\beta)^2\right)\right] \quad (3.138)$$

Finally, using Equation 3.134 and Equation 3.126 together, $\hat{p}_x$ can be written as a function of only Z and $\hat{q}$ as

$$\hat{p}_x = \frac{-N_5 Z_{xxx} - N_5 Eb\left[\frac{\varepsilon}{2}\left(\left(c - \frac{\alpha}{\alpha+\beta}\right)^2\right)_x - \frac{\varepsilon^\star}{2}\left(\left(c^\star - \frac{1}{\alpha+\beta}\right)^2\right)_x\right]}{N_5 + N_6} + \frac{N_B - N_7(q_0 + \hat{q})}{N_5 + N_6} \quad (3.139)$$

Equation 3.134 relates $\hat{p}_x^\star$ to $\hat{p}_x$, Equation 3.133 relates a to $\hat{p}_x^\star$ and $\hat{p}_x$, and Equation 3.128 gives $a^\star$ as a function of $\hat{p}_x^\star$ and $\hat{p}_x$. Therefore, now all variables are known as functions of the interface position and the surface charge density. Last equation is the other equality in Equation 3.94

$$\hat{w} - (\hat{u} + u_0)\, Z_x = Z_t \tag{3.140}$$

which can be written as

$$Z_t + \left[\frac{(Z+1)^2}{2} \left(a + \frac{\hat{p}_x}{3} (Z-2) \right) \right]_x + u_0 Z_x = 0 \tag{3.141}$$

At this point, it is not possible to advance analytically any further. Equations 3.104 and 3.141 form a set of coupled nonlinear partial differential equations. They are solved in the next section, Section 4.

4. RESULTS AND DISCUSSION

This section presents the results and their discussions. First, the tests to validate the numerical procedure and the code are presented. Then the effects of the base flow, the electric number Eb, the depth ratio β, the viscosity ratio λ, the dimensionless number S and the conductivity ratio α are examined.

4.1. Numerical Procedure

The evolution equations (Equation 3.104 and Equation 3.141) for the interface position Z and the surface charge density q present coupled nonlinear partial differential equations in space and time. The numerical procedure includes the use of fast Fourier transform (fft) and inverse fast Fourier transform (ifft) subroutines of MATLAB R2015b. To deal with the spatial derivative, Fourier transform is applied by using the eigenvalues of the Fourier derivative matrix given in [74] instead of composing and using the derivative matrix itself. Using the transform, spatial derivative of a function can be written as

$$F(f_x) = ikF(f) \tag{4.1}$$

or

$$f_x = F^{-1}\left(ikF(f)\right) \tag{4.2}$$

where F and F^{-1} represent Fourier transform and its inverse transform, k is the eigenvalues of the Fourier derivative matrix [74], i is the imaginary unit and f is an arbitrary x-dependent function. Then, Equations 3.141 and 3.104 are written as

$$Z_t = -F^{-1}\left(ikF\left(f_1\right)\right) - u_0 F^{-1}\left(ikF\left(Z\right)\right) \tag{4.3}$$

and

$$q_t = -F^{-1}\left(ikF\left(f_2\right)\right) + f_3 \tag{4.4}$$

where,

$$f_1 = \left[\frac{\left(Z+1\right)^2}{2}\left(a + \frac{\hat{p}_x}{3}\left(Z-2\right)\right)\right] \tag{4.5}$$

$$f_2 = \left[\left(u_0 + \hat{u}\right)\left(q_0 + \hat{q}\right)\right] \tag{4.6}$$

and

$$f_3 = S\left(\alpha c^\star - c\right) \tag{4.7}$$

All other spatial derivatives are also discretized using the relation given in Equation 4.2. The discretization of the time derivatives is done by using the 4^{th} order Runge-Kutta formulation [75]. In each time step, the right hand sides of Equations 4.3 and 4.4 are calculated to relate the next time step to the previous one using

$$Z_{j+1} = Z_j + \frac{\Delta t}{6}\left(Z_a + 2Z_b + 2Z_c + Z_d\right) \tag{4.8}$$

and

$$q_{j+1} = q_j + \frac{\Delta t}{6}\left(q_a + 2q_b + 2q_c + q_d\right) \tag{4.9}$$

where, j denotes j^{th} time step, Δt is the size of the time step. Z_a, Z_b, Z_c and Z_d are right hand side of Equation 4.3 evaluated at

$$Z = Z_j \tag{4.10}$$

$$Z = Z_j + Z_a \Delta t/2 \tag{4.11}$$

$$Z = Z_j + Z_b \Delta t/2 \tag{4.12}$$

and

$$Z = Z_j + Z_c \Delta t \tag{4.13}$$

respectively. q_a, q_b, q_c and q_d are calculated using the right hand side of Equation 4.3 and same relations as Z_j.

To observe the evolution of the interface, it is disturbed from its initial flat state using initial conditions in the form of

$$Z(x, 0) = A\cos(Bx) \tag{4.14}$$

where A is a small number and B is the wavenumber of the disturbance. Depending on the value of B, the interface may deflect. The critical value of B for different configurations are presented in [21, 29, 32, 33, 46] by applying linear stability analysis. The surface charge density itself is not disturbed, but affected by the disturbance on the interface. Time stepping is continued until a steady-state is reached. Since there is a base flow in the x direction, a steady-state is never reached in this direction, but a steady-state can be reached in the z direction and hereafter steady-state discussions will be on the z direction only. To check the steady-state, the amplitude of the interface, which is here defined as the vertical distance between the maximum and the minimum points of the interface is observed. When the amplitude reaches a steady-state, the interface position and the surface charge density profiles reach steady-states too.

The code starts with the inputs such as the dimensionless numbers, the number of grid points, the time step and the length of the domain, and vector k is formed.

Then the interface is disturbed using the initial condition. The main section of the code includes advancing in time using the 4^{th} order Runge-Kutta formulation.

Some difficulties were encountered during the coding process. The most important one is that the numerical configuration allows only very small time step sizes. Most of the time, these time step sizes are on the order of magnitude of 10^{-5} or 10^{-6} and advancing several millions of time steps until reaching a steady-state is very usual. Also, due to the time discretization, all equations are calculated four times per unknown, eight times in total, in each time step. Consequently, several hours of run time for each parameter set is required to reach the steady-state. To reduce the run time, the code itself can be optimized or the initial disturbance could be changed, e.g. it may be a combination of several disturbances, but in this work an efficient way of doing this could not be achieved.

As the depth ratio β is increased, some other difficulties emerged. An increase in the depth ratio means an increase in the total width of the channel, due to the scaling. This increase in the width prolongs the run time even more. Also linear stability analysis [21, 29] indicates that as β increases smaller wavenumbers should be used to deflect the interface. Some numerical experiments were done in the absence of the base flow for the default parameter set, which is given later in this section, and β=2. Those experiments showed that even disturbances with very small wavenumbers, which should deflect the interface according to the linear stability analysis, may not deflect the interface when the domain length is 2π. A possible reason might be that some key elements of the disturbance, which may be the cause of the deflection of the interface, is not included in the initial disturbance, since for small wavenumbers the period of the disturbance is much larger than the domain, which is 2π. Enlarging the domain, e.g. to 12π solves the problem, but result in another one. Since Fourier derivative matrix is defined for a domain length of 2π, when the length of the domain is changed, the code yields erroneous results. To overcome this problem, eigenvalues of the Fourier derivative matrix k should be scaled, i.e. divided by the length of the domain over 2π. Next the validation of the numerical procedure and the code is presented.

4.2. Validation

For the validation, first the results of [29] are recovered. Then three other tests are done in the presence of the base flow. Craster and Matar [29] have a similar work, in which the pressure-driven base flow is not present, i.e. the base state is stationary. As a first way of validating the formulation and the code, the results of [29] are reproduced. There are differences in the scaling between this work and [29], e.g. the electric number Eb does not emerge in [29], whereas there is no capillary number here. To recover the results, the values of the parameters in [29] are adjusted to the configuration in this work and selected as the default values of the parameters; Eb=1, β=0.5, λ=1, S=10^4, α=0.1, ε=4 and $\varepsilon^\star$=3, and the A and B in the initial condition are -0.01 and 0.01, respectively. Also, since the base state is stationary u_0 and $u_0^\star$ were set to zero. Figure 4.1 shows a sample of the reproduced results (Figure 5a in [29]). It is not possible to compare the results numerically, but by observation only, it can be concluded that the shapes and the amplitudes of the interface position and the surface charge density profiles are very similar. Hence, the code works properly when there is no base-flow.

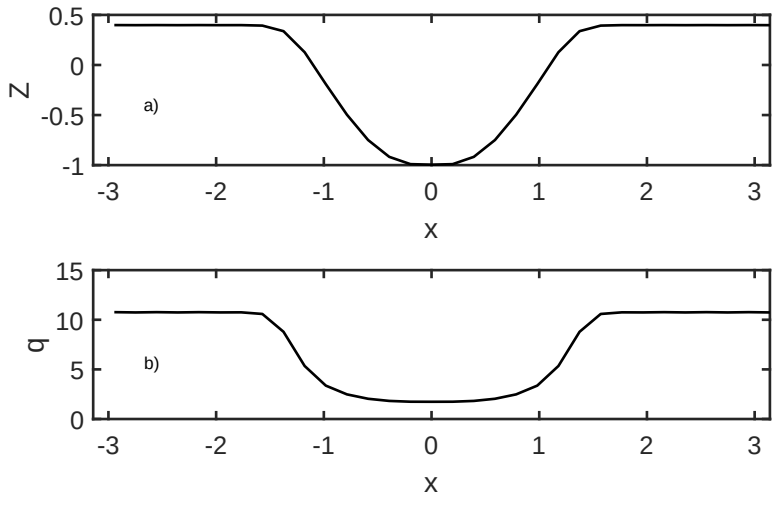

Figure 4.1. Steady-state profile of a)the interface position and b)the surface charge density in the absence of the base flow.

Next, the code and the formulation are validated in the presence of the pressure-driven base flow. In this case, three other tests are applied. First, by keeping every parameter same, the numerical procedure is started with two different initial conditions

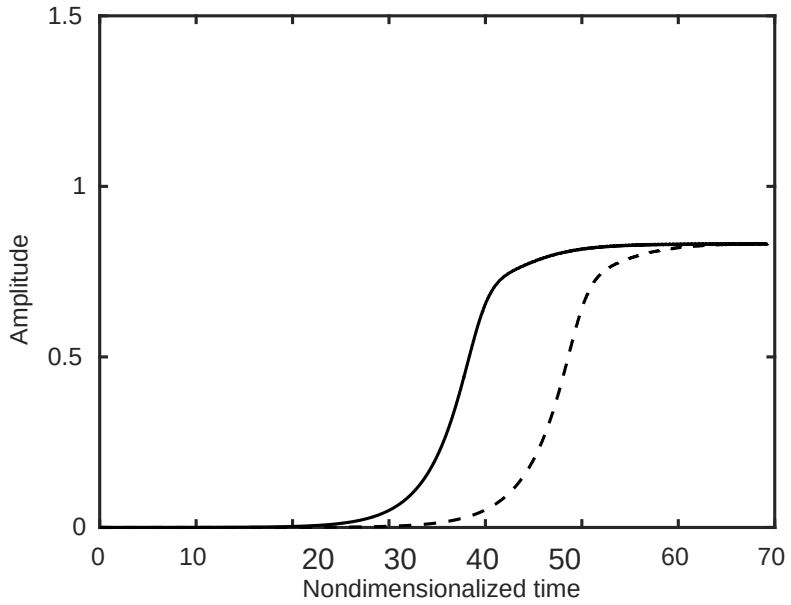

Figure 4.2. Amplitude of the interface starting with two different initial conditions.

and steady-state behaviors are observed. In Figure 4.2, the default parameter set is used and the amplitude of the interface is plotted. Here, the amplitude of the interface, defined as the vertical difference between the maximum and the minimum of the interface, is accepted as an indicator of the evolution of the interface. As expected the amplitudes of the interface reach the same point and same steady-states are obtained. Then, a second test is applied, in which the interface was disturbed one more time once it reached the steady-state. Figure 4.3 shows the amplitude of the interface after it reached steady-state and then, the interface is disturbed around t=580. As expected the disturbance dies out and the steady-state value of the amplitude of the interface is recovered. Note that the line in Figure 4.3 look very thick, but this is due to the oscillations in the amplitude. Those oscillations occur, because there is a bulk flow in the x-direction and the grid points are stationary. Therefore it is not possible to capture the real vertical maximum or the vertical minimum values of the interface in every time step, e.g. the maximum of the interface may be between two grid points. Consequently, this result, which contains oscillation having very small amplitude and period, seems like a thick line. Third test is a very simple test but an important one.

In this validation, the direction of the base state velocity is changed by keeping everything constant including the magnitude (strength) of the base flow. First, the code is run without any changes, meaning that the base flow is in positive x direction and then it is run once more, in which the direction of the base flow is changed to negative x direction simply by multiplying the base state velocity profiles with -1. The resulting steady-state interface position profiles can be seen in Figure 4.4. As expected, those two runs yield exactly symmetric with respect to steady-state interface position profiles. The amplitude of the profiles are also checked, but not presented here since they are indistinguishable. The code and the formulation managed to pass all tests mentioned here and it is concluded that the code is working properly.

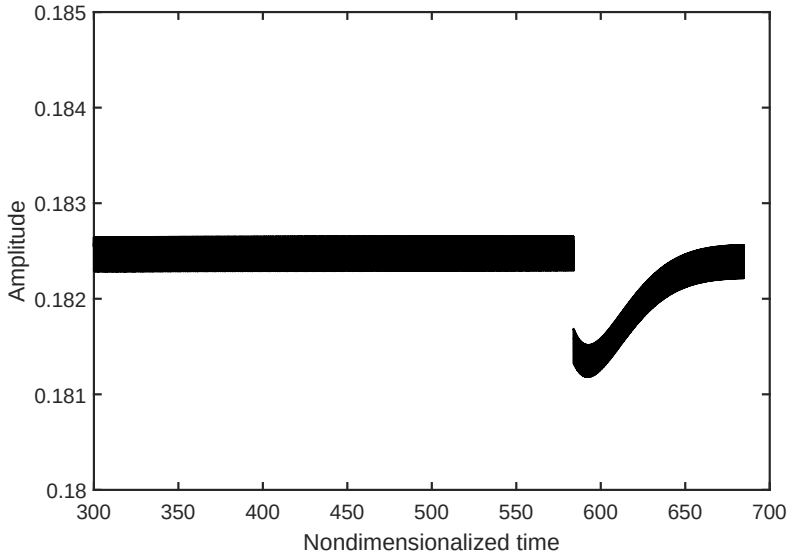

Figure 4.3. Amplitude of the interface reaches the same steady-state after a second disturbance.

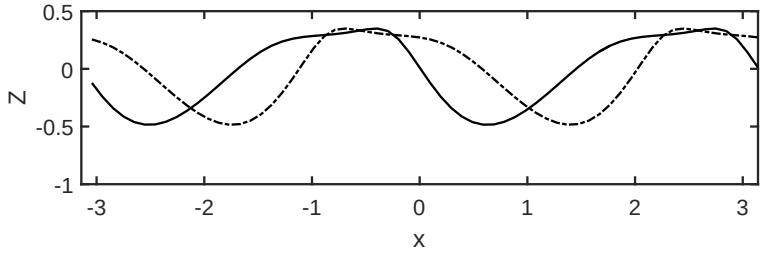

Figure 4.4. Steady-state interface position profile obtained using base state velocities of same magnitude at positive x direction (solid-line) and negative x direction (dashed-line).

4.3. Effect of the Base Flow

The effect of the base flow on the evolution of the interface can be investigated in two manners. First, the effect of the presence of the base flow and then, the effect of the strength of the base flow is examined. The nonlinear evolution of the interface in the presence of the pressure-driven base flow for the default values of the parameters is given in Figure 4.5. Two important observations can be made in the presence of the base flow. First, although the interface touches the wall (in numerical simulation it can not actually touch the wall, but it reaches to z=−0.999, where the wall is at z=-1. Therefore it can be accepted that the interface flaps the wall.) for the default values of the parameters when the base state is stationary, in the presence of the pressure-driven base flow, the interface does not reach the walls of the channel; instead a steady-state profile, which is relatively far from the walls, is observed. Second, after the initial disturbance, for a certain time, the disturbance grows but the interface remains almost perfectly symmetric. Then, as the interface moves further away from the position of the flat interface, i.e. z=0, it becomes more asymmetric.

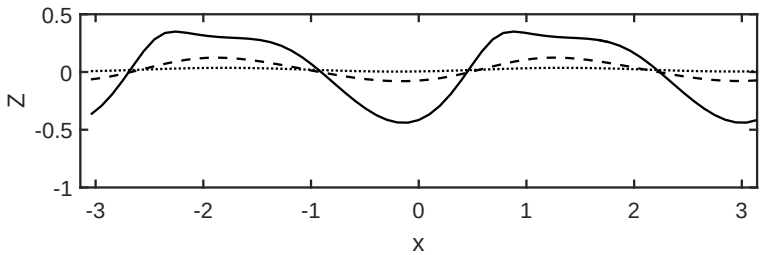

Figure 4.5. Time evolution of the interface.

Next, the effect of the strength of the base flow, which can be related to the total volumetric flow rate in the channel, is inspected. Although it can easily be changed in an experiment, here it can not be manipulated directly due to the scaling. Therefore, the base state velocity profiles are multiplied with an artificial term (u_{mult}), which is an indicator of the strength of the base flow. Figures 4.6 and 4.7 show the interface position Z and the surface charge density q for different u_{mult} values, respectively. The presence of the base flow results in a deviation from the symmetric shape of the interface attained when there is no base flow (Figure 4.6a) and increasing the strength of the base

flow yields more asymmetric shapes. This effect of u_{mult} can be observed in Figure 4.7 more clearly, where the symmetry of the surface charge density profiles changes more dramatically with the strength of the base flow. By minimizing the strength of the base flow, it is possible to asymptotically reach the steady-state interface position profile of the stationary base state case. Also, decreasing u_{mult} results in steady-state profiles that are closer to the channel wall. It can be concluded that troughs and crests of the interface position and the surface charge density coincide, by considering Figures 4.6 and 4.7 together. As shown in [21, 33], the linear stability point is not affected by the base pressure-driven flow. Therefore, at least in the early stages of the nonlinear evolution of the interface, the profiles should be similar. To verify this claim, the amplitude of the interface is plotted at different velocities in Figure 4.8. As can be se-

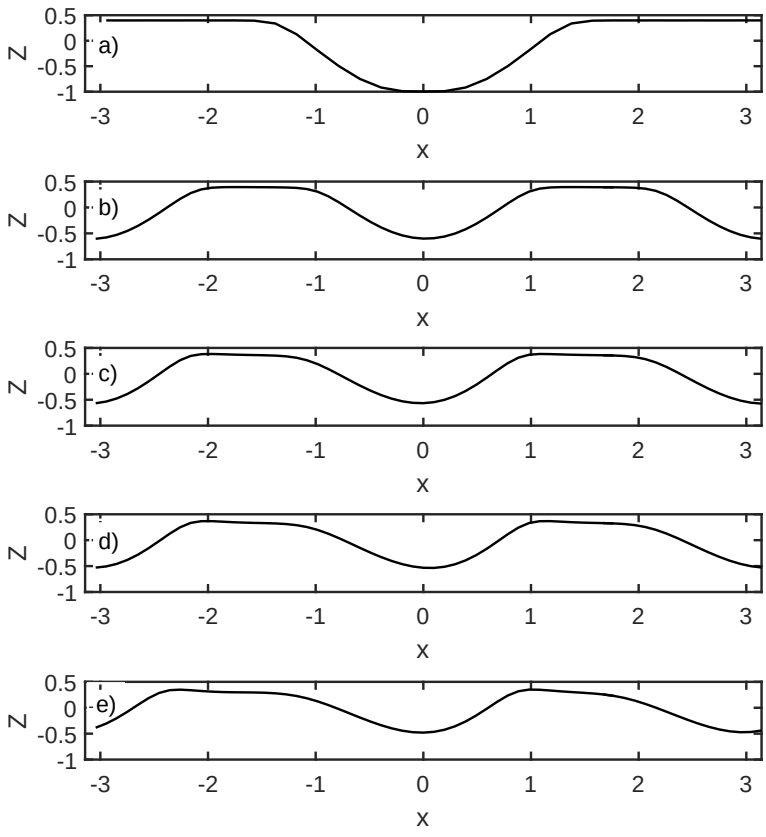

Figure 4.6. Effect of the strength of the base flow on the interface position at steady-state. Base state velocity profiles are multiplied with u_{mult} a)0 (i.e. Stationary base state), b)0.1, c)0.5, d)0.75 and e)1.

en in Figure 4.8, starting from an identical initial condition, the amplitudes follow the same curve until the late stages of the evolution.

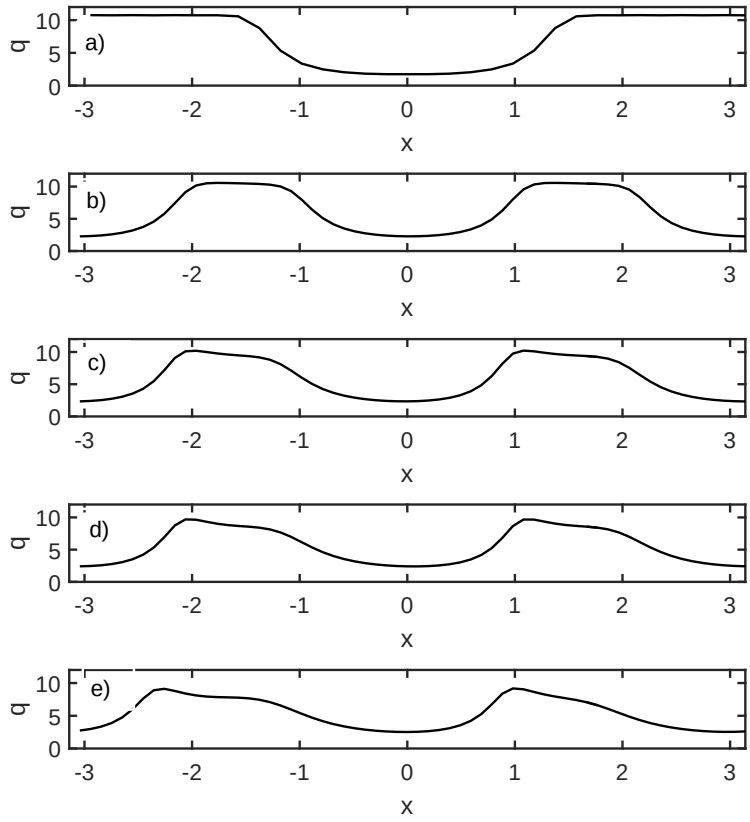

Figure 4.7. Effect of the strength of the base flow on the surface charge density at steady state. Base state velocity profiles are multiplied with u_{mult} a)0 (i.e. Stationary base state) b)0.1, c)0.5, d)0.75 and e)1.

An additional investigation is made by deleting the $u_0 Z_x$ term in Equation 3.141, but keeping all of the other base state velocity related terms. The aim here is to observe the effect of the deleted term, since it directly emerges in Equation 3.141. The amplitudes of the interface for three cases are given in Figure 4.9. The dotted curve is for the amplitude of the interface when the pressure-driven base flow is present, the dashed one is the amplitude for the stationary base state, and the solid one is for the case, in which the pressure driven base flow is present but only the $u_0 Z_x$ term is missing. It can be seen that the dashed and solid amplitudes reach the same steady-state even

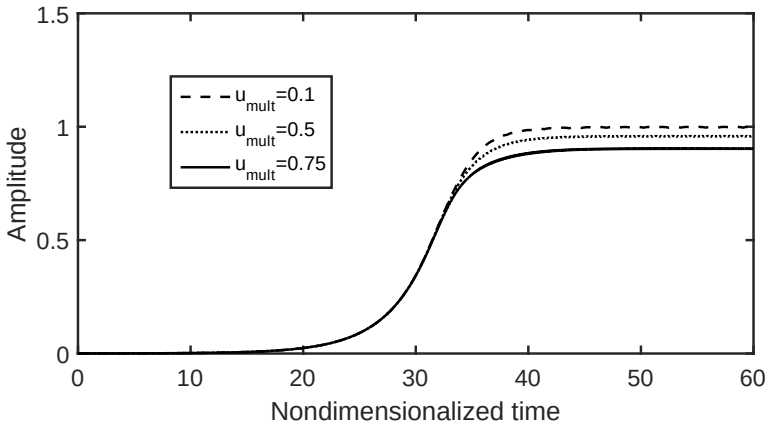

Figure 4.8. Amplitude of the interface at different velocities.

starting with different initial conditions, whereas the dotted curve reaches steady-state in a completely different amplitude. When the dashed and the solid amplitudes, start with the same initial condition, they are almost indistinguishable. Therefore, for easier observation they are started with different initial conditions. Also, the interface position profiles for the stationary and the missing term cases, are almost identical (The interface position profile is given in Figure 4.1a for the stationary base state case.); therefore the profiles are not given again. Similarly, q profiles for these two cases are also same. It can be concluded that $u_0 Z_x$ term arising from the kinematic condition is the most important term here and it causes the difference between the profiles when the pressure-driven base flow is absent and present. Other base state velocity terms emerged in the model are negligible.

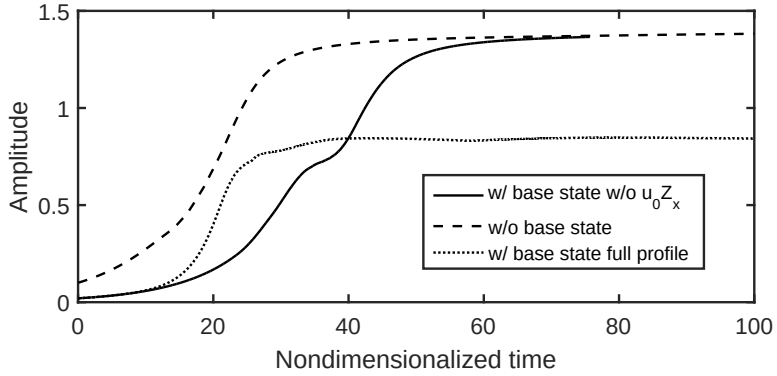

Figure 4.9. Amplitude of the interface for three cases. Solid, dashed and dotted curves represents the cases where $u_0 Z_x$ term is missing in the presence of the base flow, the base state is stationary and the base flow is present, respectively.

4.4. Effect of the Electric Number

The effect of the applied voltage on the system can be directly seen by monitoring the effect of the dimensionless electric number, defined in Equation 3.41. Therefore, it is the next important parameter to examine. The steady-state profiles of the interface position and the surface charge density for different Eb values are shown in Figures 4.10 and 4.11, respectively. According to the linear stability analysis [29], the applied voltage is destabilizing for this given set of parameters and at some critical voltage, the interface becomes unstable [21,31,32]. Therefore, it may be anticipated that below some critical Eb the disturbed interface should return back to its flat shape in the nonlinear analysis. Also, as Eb gets larger, the deflection of the interface position and the surface charge density amplitude get larger. In this work, the critical value of the Eb is not determined but the diminishing amplitude of a stable configuration can be seen in Figure 4.12, where Eb is 0.1. As Eb is increased further, an expected behavior is observed in Figures 4.10 and 4.11. For Eb=0.25, the interface does not deflect much and remains almost flat, whereas for larger values, the interface deflects. In contrast to u_{mult}, increasing Eb results in more symmetrical shapes. There is a competition bet-

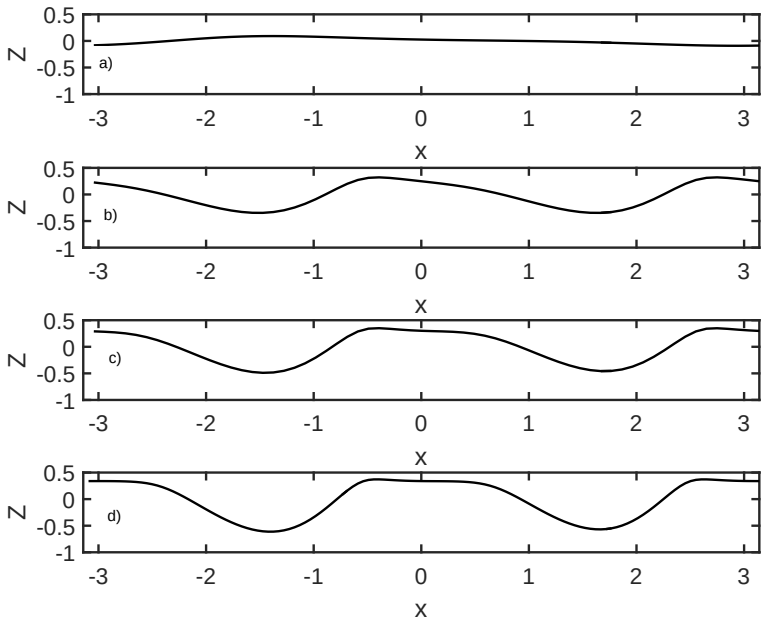

Figure 4.10. Interface position at steady-state for a)Eb=0.25, b)Eb=0.75, c)Eb=1 and d)Eb=1.25.

ween the strength of the base flow, which tends to give more asymmetric profiles with smaller steady amplitudes, and the strength of the electric field, which yields more symmetric profiles having larger amplitudes. Also, again troughs and crests of the interface position and surface charge density coincide for each Eb. As mentioned earlier, the applied voltage affects the stability according to the linear stability analysis [33]. Therefore, as expected, each amplitude in Figure 4.13 follows a separate path starting from almost right after the initial disturbance.

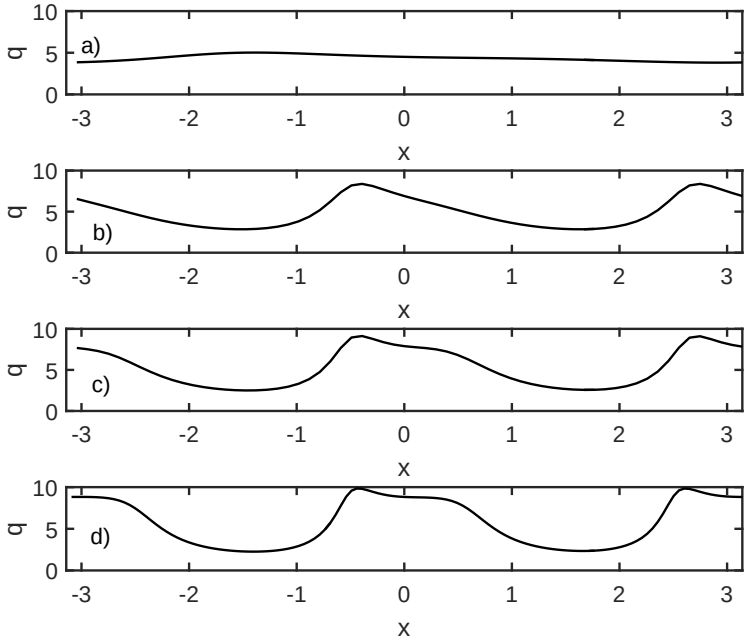

Figure 4.11. Surface charge density at steady-state for a)Eb=0.25, b)Eb=0.75, c)Eb=1 and d)Eb=1.25.

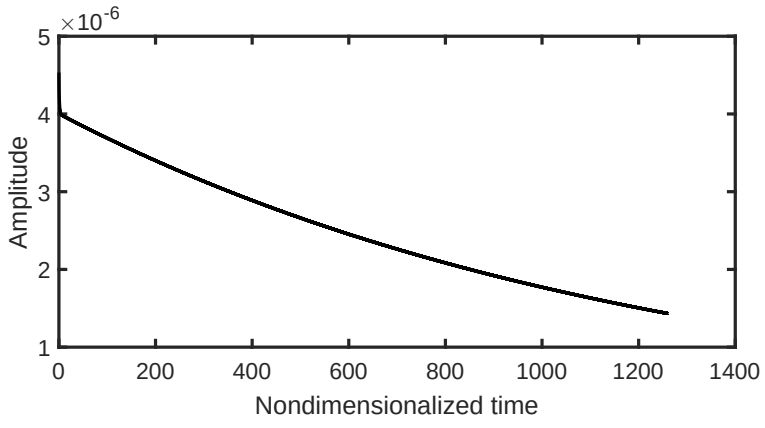

Figure 4.12. Amplitude of the stable interface for Eb=0.1.

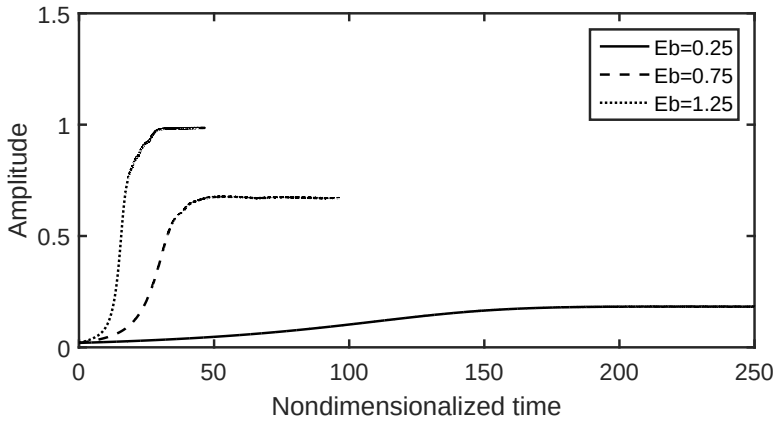

Figure 4.13. Amplitude of the interface for different Eb's.

4.5. Effect of the Depth Ratio

The depth ratio β is a function of the flow rate ratio, which is an important parameter in an experiment. The effect of the depth ratio on the interface position and the surface charge density are shown in Figures 4.14 and 4.15, respectively. As β increases, the distance between the crests of steady-state profiles of both the interface position and the surface charge density gets larger. Again, at steady-state, the troughs and the crests of the q and Z profiles for each β coincide. Another observation is that

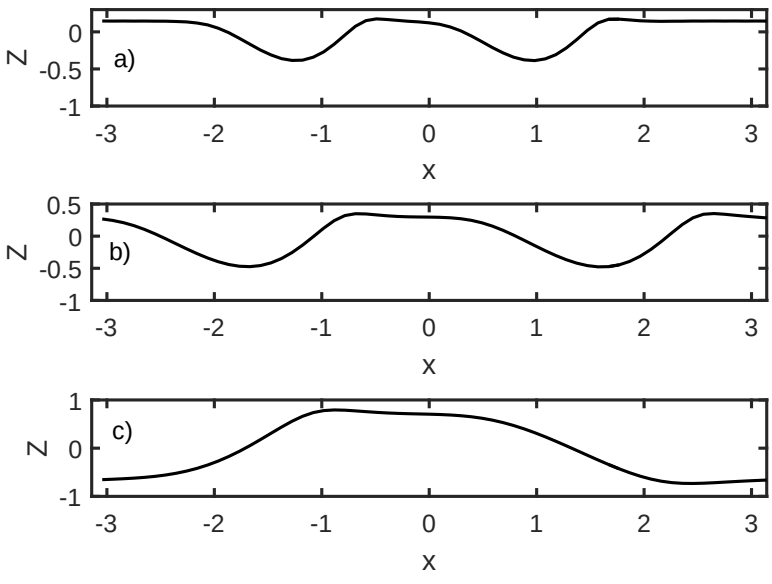

Figure 4.14. Effect of the depth ratio on the interface position at the steady-state. a) β=0.3, b) β=0.5, c) β=1.

the interface is close to the upper wall, for all three values of β given in Figure 4.14, whereas it only gets closer to the lower wall as β increases. Figure 4.15 also reveals that the values for q range between smaller values with increasing β. A similar observation is made in [29] where base pressure-driven flow is not present. This behavior can be explained using Eq. 3.74, which reveals that q_0 is inversely related to β.

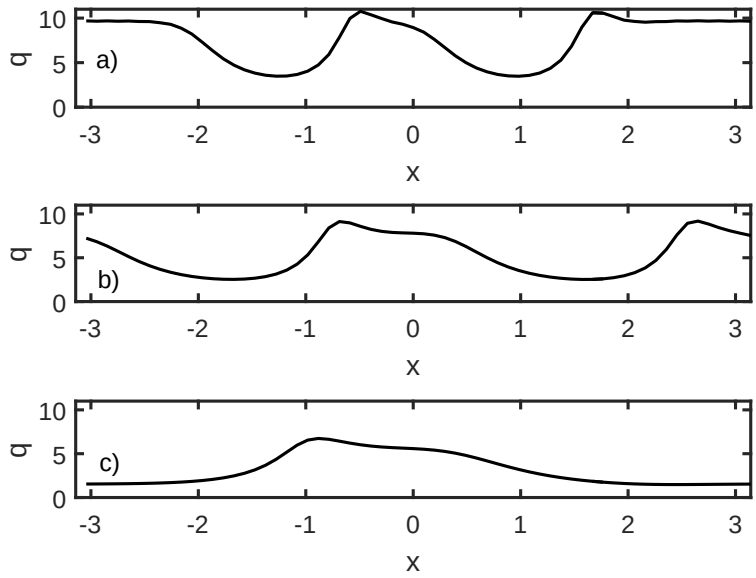

Figure 4.15. Effect of the depth ratio on the surface charge density at the steady-state. a) β=0.3, b) β=0.5, c) β=1.

Due to the scaling, as β changes the width of the channel also changes. Thus, to examine the amplitudes of the interface for different depth ratios, they are normalized by the channel width, i.e. by $1 + \beta$. The normalized amplitudes of the interface are given in Figure 4.16. First observation is that each amplitude in Figure 4.16 follows a different curve starting from the early stages, since β affects the linear stability. Also, as can be seen, β=1 has the largest normalized amplitude and as β decreases, the normalized amplitude also decreases. This observation can be explained with the effect of the strength of the base flow discussed in Section 4.3. Figure 4.17 reveals that for β=1, the maximum of the base state velocity profile is at z=0, i.e. the position of the flat interface. Since the velocity is scaled with the interface speed, the maximum value of the base state velocity is 1 for β=1. On the other hand, as shown in Figure 4.17, when β is smaller than 1, e.g. β=0.3 and β=0.5, the interface speed is smaller

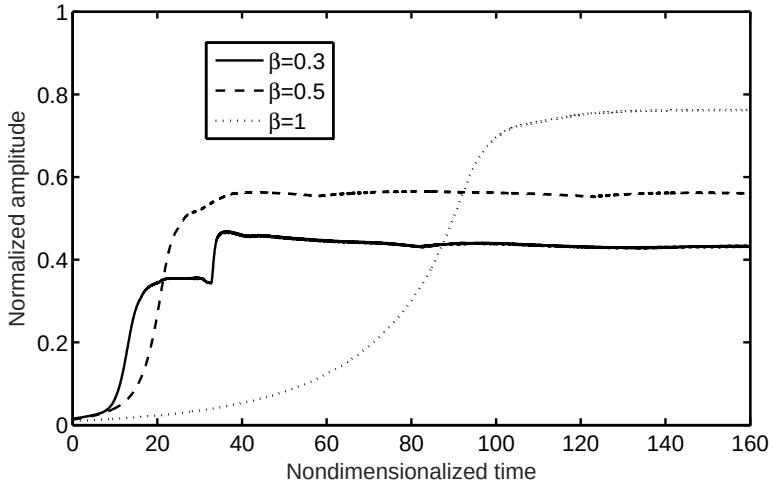

Figure 4.16. Effect of the depth ratio on the amplitude of the interface.

than the maximum of the velocity profile and after nondimensionalization, the maximum value of the velocity is greater than 1. As a result, it can be claimed that the magnitude of the velocity is greater in the latter case. The increase in the maximum point has an effect on the amplitude of the interface similar to the strength of the base flow.

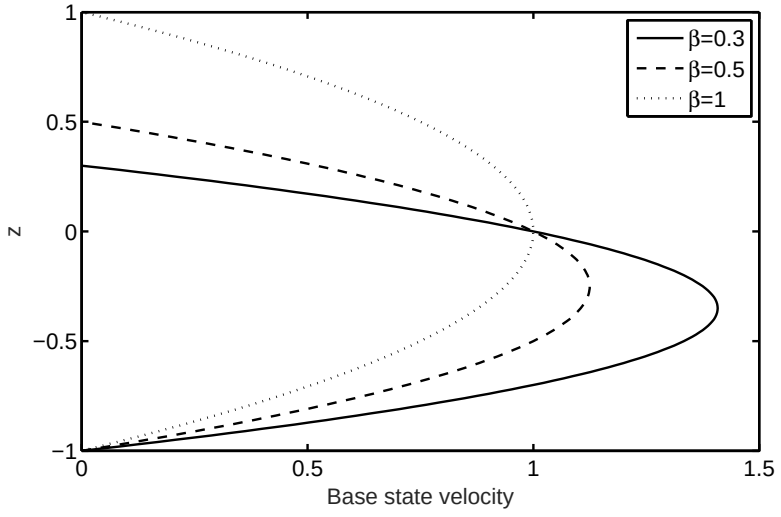

Figure 4.17. Base state velocity profiles for different β.

The claim holds when $0 < \beta < 1$, but the results for $\beta > 1$ should also be investigated. Figure 4.18 indicates that, when β is greater than 1, i.e. β=1.2, the maximum of the velocity is not on the interface and as a result the maximum speed is greater than 1. Then, with a similar reasoning, a smaller amplitude of the interface for

β=1.2 is expected. The amplitudes for β=1 and β=1.2, are presented in Figure 4.19. Although the difference is relatively small, it can be seen that the amplitude for β=1 is greater. Therefore, it is concluded that the largest amplitude of the interface occurs when the maximum of the base state velocity is at the interface. To generalize, the base state velocity profiles Equations 3.68 and 3.69 are examined. The velocity profiles reveal that the maximum velocity will be exactly on $z = 0$, when $\beta = \sqrt{\lambda}$. Therefore, keeping λ constant, the largest amplitude of the interface is observed when β=$\sqrt{\lambda}$.

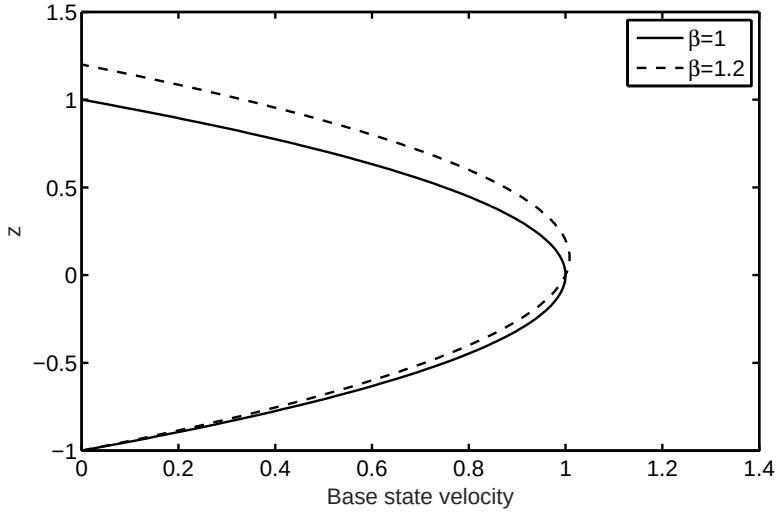

Figure 4.18. Base state velocity profiles for β=1 and β=1.2.

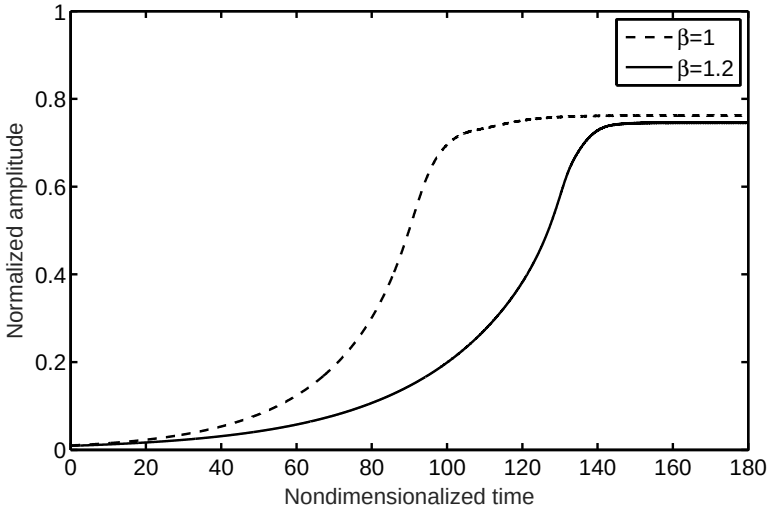

Figure 4.19. Amplitude of the interface for β=1 and β=1.2.

4.6. Effect of the Viscosity Ratio

The next dimensionless number to investigate is the viscosity ratio λ. The effect of λ on the steady-state profiles of the interface position and the surface charge density is shown in Figures 4.20 and 4.21 respectively. For each viscosity ratio value, it can be seen that the troughs and the crests of the interface position and the surface charge density coincide. Also, it is seen that an increase in λ results in more asymmetric shapes in both Z and q profiles. By considering the symmetry of the profiles, it can be said that λ has an effect similar to the strength of the base flow, i.e. increasing λ gives more asymmetric Z profiles.

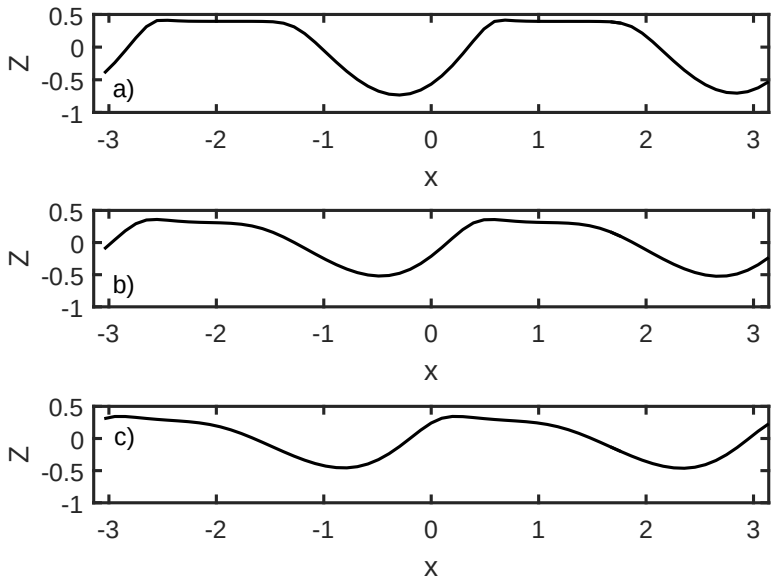

Figure 4.20. Effect of the viscosity ratio on the interface position at the steady-state. a) λ=0.25, b) λ=0.8, c) λ=1.2.

The amplitudes of the interface for $\lambda = 0.25$, $\lambda = 0.8$ and $\lambda = 1.2$ are given in Figure 4.22. As λ decreases, the amplitude of the interface gets larger. In Section 4.5, the size of the amplitude was related to the base flow and it was determined that the largest amplitude occurs for $\beta = \sqrt{\lambda}$. Since in Figure 4.22 the default values of the parameters are used, where $\beta = 0.5$, it is expected to have the largest amplitude for $\lambda = 0.25$. As expected, $\lambda = 0.25$ has the largest amplitude compared to the amplitudes for $\lambda > 0.25$. However, when $\lambda < 0.25$ is investigated, it is seen that the amplitude

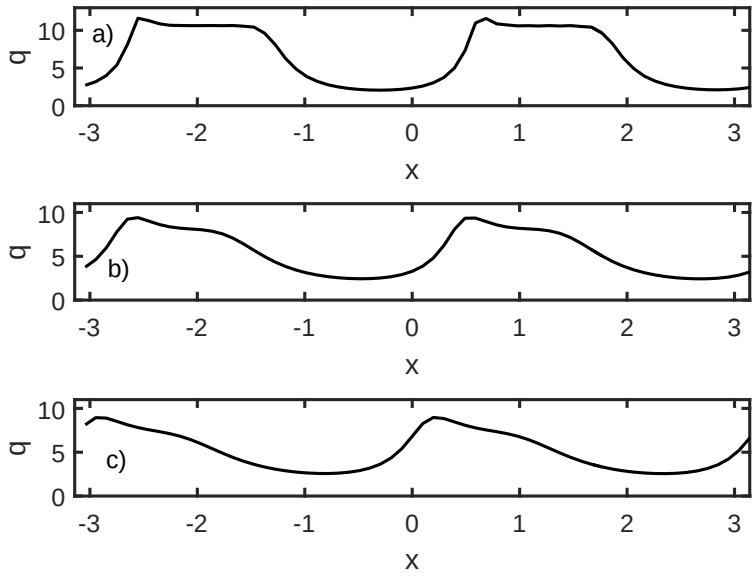

Figure 4.21. Effect of the viscosity ratio on the surface charge density at the steady-state. a) λ=0.25, b) λ=0.8, c) λ=1.2.

of the interface for $\lambda = 0.2$ is larger than $\lambda = 0.25$, which is not expected based on the analysis in Section 4.5. Therefore, it is concluded that the explanation holds when λ is constant and β is changed, i.e. for constant λ the largest amplitude occurs for $\beta = \sqrt{\lambda}$, whereas when β is constant, the largest amplitude may not be at $\lambda = \beta^2$. This conclusion may indicate that the decrease in the viscosity ratio below 0.25, has other effects on the system, which are more important than the effect of the base flow.

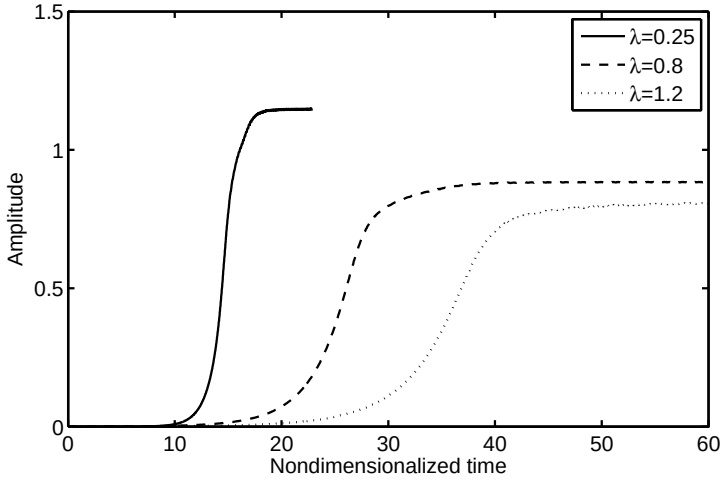

Figure 4.22. Amplitude of the interface for λ=0.25, λ=0.8 and λ=1.2.

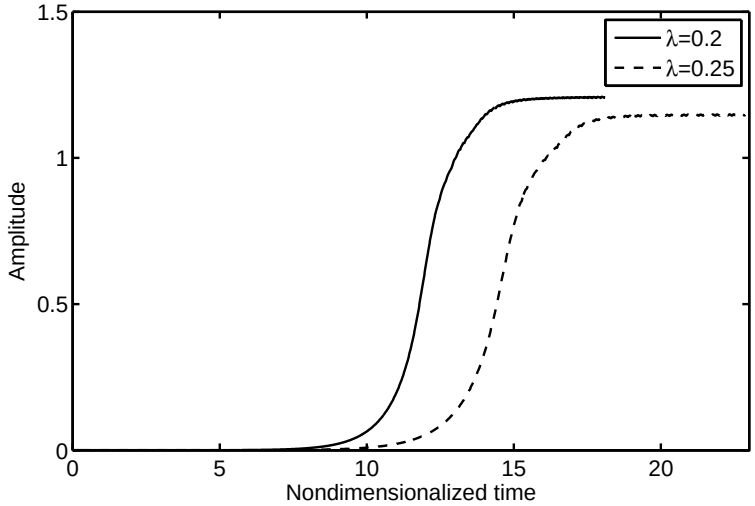

Figure 4.23. Amplitude of the interface for λ=0.2 and λ=0.25.

4.7. Effect of the Dimensionless Number S

The dimensionless number S given by Equation 3.41, shows the ratio of the fluid to electric time scales. In the case of the fast electric charge relaxation times, i.e. $S >> 1$, the perturbed equations in the linear stability analysis can be simplified and the dispersion relationship, i.e. the growth rate of the disturbance versus wavenumber,is independent of S [33]. Therefore, it is expected to observe a single behavior in the nonlinear analysis for different high S values at least in the early stages of the instability. Figure 4.24 shows that the steady-state interface position profiles for $S = 10^4$ (Figure 4.24b) and $S = 10^6$ (Figure 4.24c) are almost indistinguishable, which means that even at the end of the evolution, Z is same for different large values of S. Similarly, the surface charge density profiles can be interpreted with the help of Figures 4.25b and 4.25c. Although the Z profile for $S = 300$ (Figure 4.24a) looks similar to the others, it is slightly different. It has narrower troughs and wider crests. The difference is more obvious in q profiles. In Figure 4.25, it is seen that the crests in the q profile for $S = 300$ has a distinguishable bulge, whereas others are smoother. To reveal the differences between large and small values of S more clearly, other results where S is on the order of magnitude of 1 should be examined. However due to the numerical difficulties, these results could not be obtained in this work. A final discussion is made on the amplitude of the interface position profiles (Figure 4.26). The amplitudes for

$S = 10^6$ and $S = 10^4$ are identical as expected. Although, the amplitudes between $t = 0$ and $t \approx 50$, and after $t \approx 60$ for $S = 300$ are very similar to the others, it is seen that the behavior between $t \approx 50$ and $t \approx 60$ is different.

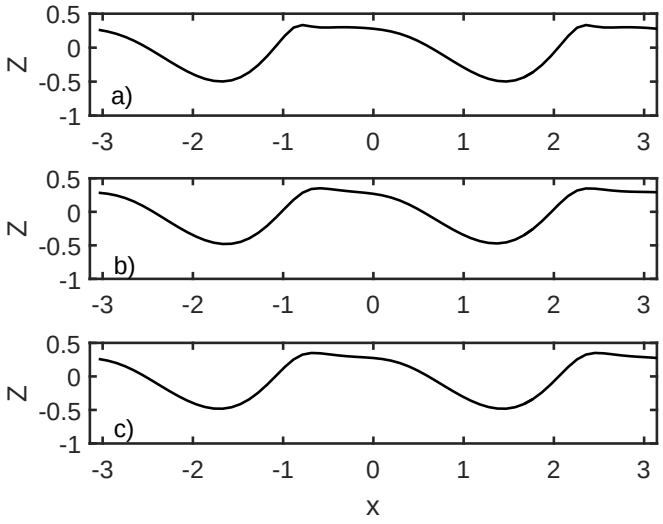

Figure 4.24. Effect of the dimensionless number S on the interface position at the steady-state. a) $S = 300$, b) $S = 10^4$, c) $S = 10^6$.

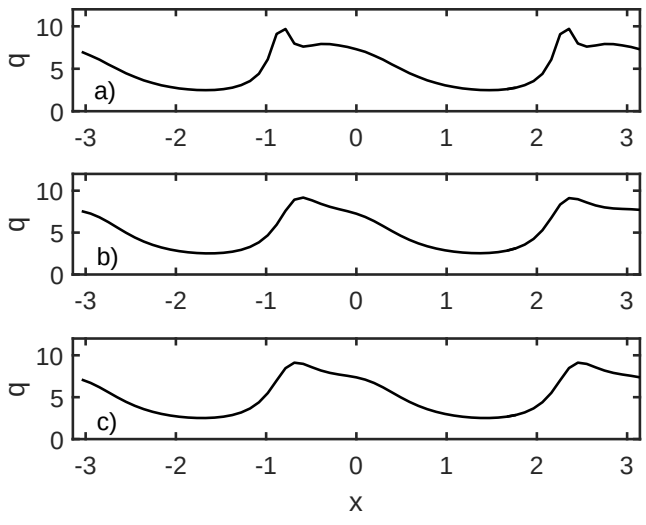

Figure 4.25. Effect of the dimensionless number S on the surface charge density at the steady-state. a) $S = 300$, b) $S = 10^4$, c) $S = 10^6$.

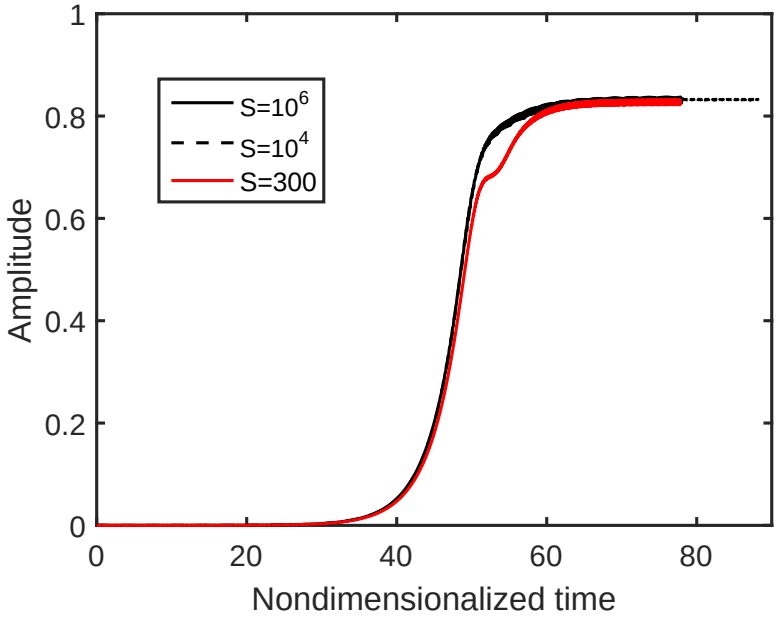

Figure 4.26. Amplitude of the interface for different S.

4.8. Effect of the Conductivity Ratio

The last dimensionless number, which is considered in this work, is the conductivity ratio α. The steady state interface position profiles for different α are given in Figure 4.27. As first three subplots of Figure 4.27 show increasing α result in slightly less symmetric interfaces whereas in Figure 4.27d it is seen that the interface remains almost flat as in Figure 4.10a. The difference between the profiles is clearer when the surface charge density profiles given in Figure 4.28 are studied. There are two peaks in each crest of the q profile for $\alpha = 0.9$ and as α is increased to 1.1 and 1.2, one of them disappears. Again, when α is 2 the q profile is almost flat. The amplitudes of the interface position at different conductivity ratios are shown in Figure 4.29. As α increases, the amplitude of the steady-state Z profile decreases and the time to reach to steady-state increases.

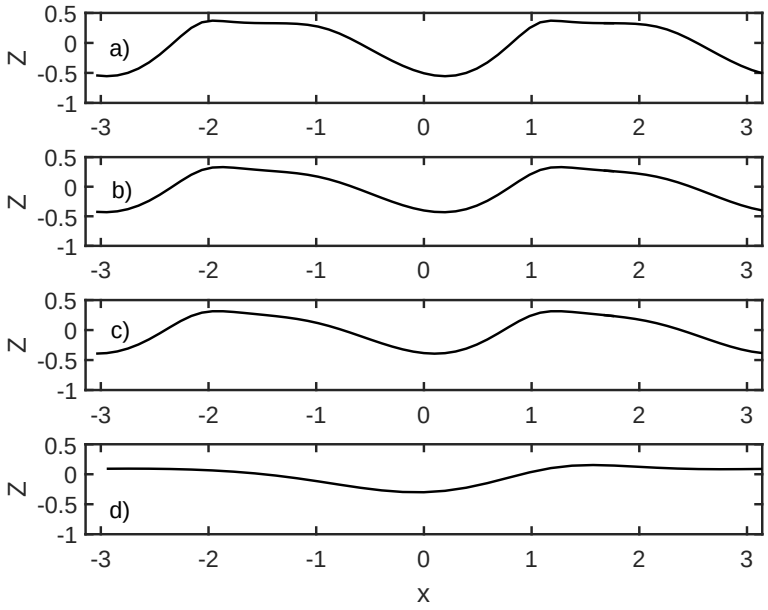

Figure 4.27. Effect of the conductivity ratio on the interface position at the steady-state. a) α=0.9, b) α=1.1, c) α=1.2 d) α=2.

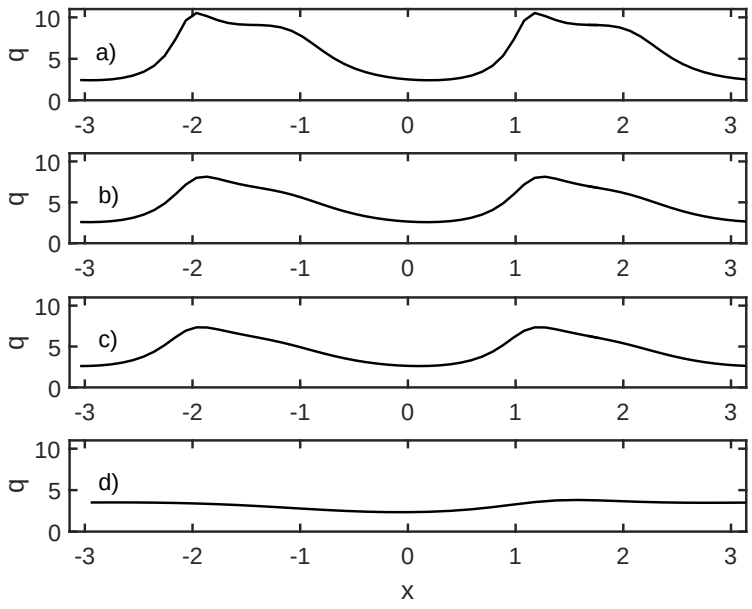

Figure 4.28. Effect of the conductivity ratio on the surface charge density at the steady-state. a) α=0.9, b) α=1.1, c) α=1.2 d) α=2.

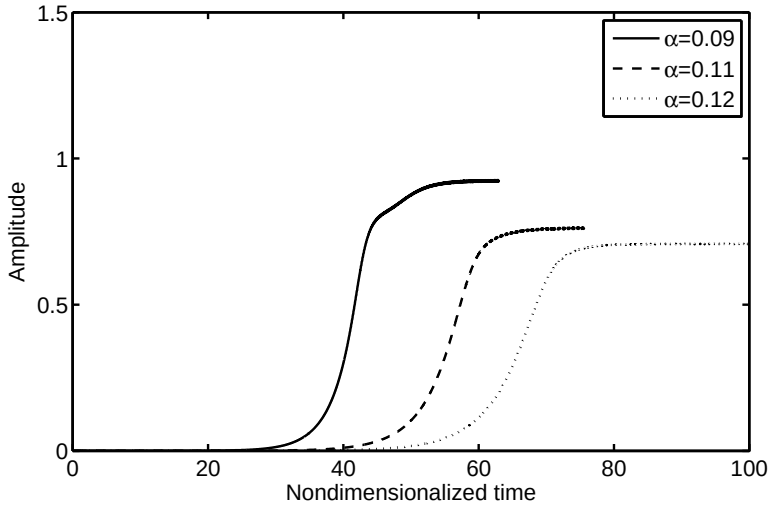

Figure 4.29. Amplitude of the interface for different conductivity ratios.

5. CONCLUSIONS AND RECOMMENDATIONS

5.1. Conclusions

In this work, the effect of the presence and the strength of a pressure-driven base flow, and the effects of the physical parameters; such as the voltage difference, the depth ratio, the viscosity ratio, the ratio of fluid to electric time scales, and conductivity ratio represented by the dimensionless numbers Eb, β, λ, S and α on the evolution of the interface position between two immiscible leaky dielectric fluids subjected to a normal electric field in a micro channel are investigated.

Presence of a pressure-driven base flow results in two major effects. First, in all configurations considered in this work, it is seen that in the presence of the base flow the interface does not reach the walls, whereas it was experimentally shown that once the interface becomes unstable, it deforms and touches the walls [39]. That difference between the experimental and the numerical results may be due to a deficiency in the model, e.g. the intermolecular forces. Second, steady-state profiles of both Z and q (Figures 4.6 and 4.7) become asymmetric in the presence of the base flow. An increase in the strength of the base flow yields more asymmetric steady-state Z and q profiles having smaller amplitudes. Also, it is shown in Figure 4.9 that the major effect of the base flow stems from the $u_0 Z_x$ term arising from the kinematic condition Eq. (3.6) and other base state related terms, such as N_B Eq. (3.136), are negligible.

As the electric number Eb increases, the Z and q profiles (Figures 4.10 and 4.11) become more symmetric and the amplitude of the interface position gets larger. The electric number and the strength of the base flow have exactly opposite effects on the profiles. Therefore, it is concluded that there is a competition between these two parameters.

When the depth ratio is considered, it is seen in Figures 4.16 and 4.19 that the largest normalized steady-state amplitude for the interface occurs when the maximum

of the base state velocity profile is on z=0, which corresponds to β=$\sqrt{\lambda}$. Also, the distance between the troughs in both Z and q (Figures 4.14 and 4.15) profiles gets larger for higher β.

Smaller viscosity ratios λ yield more symmetric Z and q profiles (Figures 4.20 and 4.21). When β is kept constant, the largest steady-state amplitude of Z does not occur for λ=β^2 (Figure 4.23), which gives the interface speed as the maximum of the base state velocity profiles. Decreasing λ further after λ=β^2, results in even larger amplitudes. Therefore, it is concluded that λ affects the system more, individually, compared to its effect via the base flow.

For large ratios of fluid to electric time scales, represented by the dimensionless number S, the steady state Z and q (Figures 4.24 and 4.25) profiles are indistinguishable. For small values of S, e.g. 300, Z profile is still similar to those of large S values. However the steady-state q profiles are significantly different. Also, although the time evolution of the interface differs between $t \approx 50$ and $t \approx 60$, for all three values of S, Z reaches the same steady-state amplitude (Figure 4.26).

Increasing the conductivity ratio α has a similar effect to decreasing the electric number. The interface position (Figure 4.27) and the surface charge density (Figure 4.28) profiles become more asymmetric for higher α values. Also, the amplitude of the steady-state Z profile (Figure 4.29) is larger for smaller conductivity ratios.

5.2. Recommendations

The theoretical results presented in this work do not match with the experiments conducted in a similar configuration [39]. The discrepancy is more pronounced at the later stages of the evolution of the interface. In the experiments the interface flaps the walls, whereas in the numerical results it reaches a steady-state before reaching the walls. Consequently to match the theory with the experiment, the mathematical model should be improved. Additional forces such as intermolecular forces may be implied in the model. An electrical Marangoni number could be obtained by adding

the dependence of the surface tension on the electric field as the magnitude of the electric field is as high as 10^6 V/m and it is known that surface tension depends on the electric field [76].

In order to lose the oscillations mentioned in Section 4.2 and to obtain more accurate results, a numerical procedure with moving meshes could be used.

Finally, different physical configurations, e.g. a configuration in which the electric field is parallel to the direction of the base flow, can be investigated.

REFERENCES

1. Whitesides, G. M., "The Origins and the Future of Microfluidics", *Nature*, Vol. 442, pp. 368–373, 2006.

2. Schwesinger, N., T. Frank and H. Wurmus, "A Modular Microfluid System with an Integrated Micromixer", *Journal of Micromechanics and Microengineering*, Vol. 6, No. 1, pp. 99–102, 1996.

3. Lin, C. H., L.-M. Fu and Y.-S. Chien, "Microfluidic T-form Mixer Utilizing Switching Electroosmotic Flow", *Analytical Chemistry*, Vol. 76, No. 18, pp. 5265–5272, 2004.

4. Stone, H., A. Stroock and A. Ajdari, "Engineering flows in small devices: Microfluidics toward a Lab-on-a-Chip", *Annual Review of Fluid Mechanics.*, Vol. 36, pp. 381–411, 2004.

5. Hosokawa, K., T. Fujii and I. Endo, "Droplet-based Nano/Picoliter Mixer Using Hydrophobic Microcapillary Vent", *Micro Electro Mechanical Systems, 1999. MEMS'99. Twelfth IEEE International Conference on*, pp. 388–393, IEEE, 1999.

6. Liu, R. H., M. A. Stremler, K. V. Sharp, M. G. Olsen, J. G. Santiago, R. J. Adrian, H. Aref and D. J. Beebe, "Passive Mixing in a Three-Dimensional Serpentine Microchannel", *Journal of Microelectromechanical Systems*, Vol. 9, No. 2, pp. 190–197, 2000.

7. Yang, J.-T., K.-J. Huang, K.-Y. Tung, I.-C. Hu and P.-C. Lyu, "A Chaotic Micromixer Modulated by Constructive Vortex Agitation", *Journal of Micromechanics and Microengineering*, Vol. 17, No. 10, pp. 2084–2092, 2007.

8. Moroney, R., R. White and R. Howe, "Ultrasonically Induced Microtransport", *Micro Electro Mechanical Systems, 1991, MEMS'91, Proceedings. An Investigation*

of Micro Structures, Sensors, Actuators, Machines and Robots. IEEE, pp. 277–282, 1991.

9. Evans, J., D. Liepmann and A. P. Pisano, "Planar Laminar Mixer", *Proc. MEMS'97, 10th IEEE Int. Workshop Micro Electromechanical System (Nagoya, Japan)*, pp. 96–101, 1997.

10. Evensen, H., D. Meldrum and D. Cunningham, "Automated Fluid Mixing in Glass Capillaries", *Review of Scientific Instruments*, Vol. 69, No. 2, pp. 519–526, 1998.

11. Nguyen, N.-T. and Z. Wu, "Micromixers—A Review", *Journal of Micromechanics and Microengineering*, Vol. 15, No. 2, pp. R1–R16, 2004.

12. Umbanhowar, P., V. Prasad and D. Weitz, "Monodisperse Emulsion Generation via Drop Break off in a Coflowing Stream", *Langmuir*, Vol. 16, No. 2, pp. 347–351, 2000.

13. Thorsen, T., R. W. Roberts, F. H. Arnold and S. R. Quake, "Dynamic Pattern Formation in a Vesicle-Generating Microfluidic Device", *Physical Review Letters*, Vol. 86, No. 18, pp. 4163–4166, 2001.

14. Anna, S. L., N. Bontoux and H. A. Stone, "Formation of Dispersions Using "Flow Focusing" in Microchannels", *Applied Physics Letters*, Vol. 82, No. 3, pp. 364–366, 2003.

15. Ozen, O., N. Aubry, D. Papageorgiou and P. Petropoulos, "Monodisperse Drop Formation in Square Microchannels", *Physical Review Letters*, Vol. 96, No. 14, pp. 144501.1–4, 2006.

16. Tan, S.-H., N.-T. Nguyen, L. Yobas and T. G. Kang, "Formation and Manipulation of Ferrofluid Droplets at a Microfluidic T-junction", *Journal of Micromechanics and Microengineering*, Vol. 20, No. 4, pp. 045004.1–10, 2010.

17. Nguyen, N.-T., T.-H. Ting, Y.-F. Yap, T.-N. Wong, J. C.-K. Chai, W.-L. Ong, J. Zhou, S.-H. Tan and L. Yobas, "Thermally Mediated Droplet Formation in Microchannels", *Applied Physics Letters*, Vol. 91, No. 8, pp. 084102.1–3, 2007.

18. Willaime, H., V. Barbier, L. Kloul, S. Maine and P. Tabeling, "Arnold Tongues in a Microfluidic Drop Emitter", *Physical Review Letters*, Vol. 96, No. 5, pp. 054501.1–4, 2006.

19. Melcher, J. R. and W. J. Schwarz Jr, "Interfacial Relaxation Overstability in a Tangential Electric Field", *Physics of Fluids*, Vol. 11, No. 12, pp. 2604–2616, 1968.

20. Saville, D., "Electrohydrodynamics: The Taylor-Melcher Leaky Dielectric Model", *Annual Review of Fluid Mechanics*, Vol. 29, No. 1, pp. 27–64, 1997.

21. Thaokar, R. M. and V. Kumaran, "Electrohydrodynamic Instability of the Interface Between two Fluids Confined in a Channel", *Physics of Fluids*, Vol. 17, pp. 084104.1–20, 2005.

22. Schäffer, E., T. Thurn-Albrecht, T. P. Russell and U. Steiner, "Electrically Induced Structure Formation and Pattern Transfer", *Nature*, Vol. 403, No. 6772, pp. 874–877, 2000.

23. Schäffer, E., T. Thurn-Albrecht, T. P. Russell and U. Steiner, "Electrohydrodynamic Instabilities in Polymer Films", *Europhysics Letters*, Vol. 53, No. 4, pp. 518–523, 2001.

24. Chou, S., L. Zhuang and L. Guo, "Lithographically Induced Self-Construction of Polymer Microstructures for Resistless Patterning", *Applied Physics Letters*, Vol. 75, pp. 1004–1006, 1999.

25. Levich, V. G., *Physicochemical Hydrodynamics*, Prentice Hall, 1962.

26. Hoburg, J. F. and J. R. Melcher, "Internal Electrohydrodynamic Instability and

Mixing of Fluids with Orthogonal Field and Conductivity Gradients", *Journal of Fluid Mechanics*, Vol. 73, pp. 333–351, 1976.

27. Melcher, J. R., *Continuum Electromechanics*, Vol. 2, MIT press Cambridge, 1981.

28. Tilley, B. S., P. G. Petropoulos and D. T. Papageorgiou, "Dynamics and Rupture of Planar Electrified Liquid Sheets", *Physics of Fluids*, Vol. 13, No. 12, pp. 3547–3563, 2001.

29. Craster, R. V. and O. K. Matar, "Electrically Induced Pattern Formation in Thin Leaky Dielectric Films", *Physics of Fluids*, Vol. 17, No. 3, pp. 032104.1–17, March 2005.

30. Zahn, J. D. and V. Reddy, "Two Phase Micromixing and Analysis Using Electrohydrodynamic Instabilities", *Microfluid Nanofluid*, Vol. 2, pp. 399–415, 2006.

31. Ozen, O., N. Aubry, D. Papageorgiou and P. Petropoulos, "Electrohydrodynamic Linear Stability of Two Immiscible Fluids in Channel Flow", *Electrochimica Acta*, Vol. 51, pp. 5316–5323, 2006b.

32. Uguz, A. K., O. Ozen and N. Aubry, "Electric Field Effect on a Two-Fluid Interface Instability in Channel Flow for Fast Electric Times", *Physics of Fluids*, Vol. 20, pp. 031702.1–4, 2008.

33. Uguz, A. K. and N. Aubry, "Quantifying the Linear Stability of a Flowing Electrified Two-Fluid Layer in a Channel for Fast Electric Times for Normal and Parallel Electric Fields", *Physics of Fluids*, Vol. 20, No. 9, pp. 092103.1–10, 2008.

34. O'Konski, C. T. and H. C. Thacher Jr, "The Distortion of Aerosol Droplets by an Electric Field", *The Journal of Physical Chemistry*, Vol. 57, No. 9, pp. 955–958, 1953.

35. Allan, R. and S. Mason, "Particle Behaviour in Shear and Electric Fields. I. De-

formation and Burst of Fluid Drops", *Proceedings of the Royal Society of London A: Mathematical, Physical and Engineering Sciences*, Vol. 267, pp. 45–61, 1962.

36. Taylor, G., "Studies in electrohydrodynamics. I. The circulation produced in a drop by electrical field", *Proceedings of the Royal Society of London A: Mathematical, Physical and Engineering Sciences*, Vol. 291, pp. 159–166, 1966.

37. Melcher, J. R. and G. I. Taylor, "Electrohydrodynamics: A Review of Role of Interfacial Shear Stresses", *Annual Review of Fluid Mechanics*, Vol. 1, pp. 111–146, 1969.

38. Li, F., O. Ozen, A. Aubry, D. T. Papageorgiou and P. G. Petropoulos, "Linear Stability of a Two-Fluid Interface for Electrohydrodynamic Mixing in a Channel", *Journal of Fluid Mechanics*, Vol. 583, pp. 347–377, 2007.

39. Eribol, P. and A. Uguz, "Experimental Investigation of Electrohydrodynamic Instabilities in Micro Channels", *European Physical Journal Special Topics*, Vol. 224, pp. 423–432, 2016.

40. Hoburg, J. and J. Melcher, "Electrohydrodynamic Mixing and Instability Induced by Co-Linear Fields and Conductivity Gradients", *Physics of Fluids*, Vol. 20, No. 6, pp. 903–911, 1977.

41. Baygents, J. C. and F. Baldessari, "Electrohydrodynamic Instability in a Thin Fluid Layer with an Electrical Conductivity Gradient", *Physics of Fluids*, Vol. 10, No. 1, pp. 301–311, 1998.

42. Oddy, M., J. Santiago and J. Mikkelsen, "Electrokinetic Instability Micromixing", *Analytical Chemistry*, Vol. 73, No. 24, pp. 5822–5832, 2001.

43. El Moctar, A. O., N. Aubry and J. Batton, "Electro-Hydrodynamic Micro-Fluidic Mixer", *Lab on a Chip*, Vol. 3, No. 4, pp. 273–280, 2003.

44. Posner, J. D. and J. G. Santiago, "Convective Instability of Electrokinetic Flows in a Cross-Shaped Microchannel", *Journal of Fluid Mechanics*, Vol. 555, pp. 1–42, 2006.

45. Lin, H., "Electrokinetic Instability in Microchannel Flows: A Review", *Mechanics Research Communications*, Vol. 36, No. 1, pp. 33–38, 2009.

46. Shankar, V. and A. Sharma, "Instability of the Interface Between Thin Fluid Films Subjected to Electric Fields", *Journal of Colloid and Interface Science*, Vol. 274, No. 1, pp. 294–308, 2004.

47. Papageorgiou, D. and P. Petropoulos, "Generation of Interfacial Instabilities in Charged Electrified Viscous Liquid Films", *Journal of Engineering Mathematics*, Vol. 50, No. 2-3, pp. 223–240, 2004.

48. Roberts, S. A. and S. Kumar, "AC Electrohydrodynamic Instabilities in Thin Liquid Films", *Journal of Fluid Mechanics*, Vol. 631, pp. 255–279, 2009.

49. Gambhire, P. and R. Thaokar, "Electrohydrodynamic Instabilities at Interfaces Subjected to Alternating Electric Field", *Physics of Fluids*, Vol. 22, No. 6, pp. 064103.1–16, 2010.

50. Maehlmann, S. and D. T. Papageorgiou, "Interfacial Instability in Electrified Plane Couette Flow", *Journal of Fluid Mechanics*, Vol. 666, pp. 155–188, 2011.

51. Esmaeeli, A. and M. N. Reddy, "The Electrohydrodynamics of Superimposed Fluids Subjected to a Nonuniform Transverse Electric Field", *International Journal of Multiphase Flow*, Vol. 37, No. 10, pp. 1331–1347, 2011.

52. Ramkrishnan, A. and S. Kumar, "Electrohydrodynamic Effects in the Leveling of Coatings", *Chemical Engineering Science*, Vol. 101, pp. 785–799, 2013.

53. Ramkrishnan, A. and S. Kumar, "Electrohydrodynamic Deformation of Thin Liq-

uid Films near Surfaces with Topography", *Physics of Fluids*, Vol. 26, No. 12, pp. 122110.1–18, 2014.

54. Corbett, A. and S. Kumar, "Combined Thermal and Electrohydrodynamic Patterning of Thin Liquid Films", *Journal of Engineering Mathematics*, Vol. 94, No. 1, pp. 81–96, 2015.

55. Young, Y.-N. and M. J. Miksis, "Electrohydrodynamic Instability of a Capacitive Elastic Membrane", *Physics of Fluids*, Vol. 27, No. 2, pp. 022102.1–19, 2015.

56. Lanauze, J. A., L. M. Walker and A. S. Khair, "Nonlinear Electrohydrodynamics of Slightly Deformed Oblate Drops", *Journal of Fluid Mechanics*, Vol. 774, pp. 245–266, 2015.

57. Kochurin, E. A. and N. M. Zubarev, "Reduced Equations of Motion of the Interface of Dielectric Liquids in Vertical Electric and Gravitational Fields", *Physics of Fluids*, Vol. 24, No. 7, pp. 072101.1–17, 2012.

58. Karapetsas, G. and V. Bontozoglou, "Non-Linear Dynamics of a Viscoelastic Film Subjected to a Spatially Periodic Electric Field", *Journal of Non-Newtonian Fluid Mechanics*, Vol. 217, pp. 1–13, 2015.

59. Kourmatzis, A. and J. S. Shrimpton, "Characteristics of Electrohydrodynamic Roll Structures in Laminar Planar Couette Flow", *Journal of Physics D: Applied Physics*, Vol. 49, No. 4, pp. 045503.1–13, 2015.

60. Herminghaus, S., "Dynamical Instability of Thin Liquid Films between Conducting Media", *Physical Review Letters*, Vol. 83, No. 12, pp. 2359–2361, 1999.

61. Tseluiko, D. and D. T. Papageorgiou, "Nonlinear Dynamics of Electrified Thin Liquid Films", *SIAM Journal on Applied Mathematics*, Vol. 67, No. 5, pp. 1310–1329, 2007.

62. Tseluiko, D., M. Blyth, D. Papageorgiou and J.-M. Vanden-Broeck, "Effect of an Electric Field on Film Flow Down a Corrugated Wall at Zero Reynolds Number", *Physics of Fluids*, Vol. 20, No. 4, pp. 042103.1–19, 2008.

63. Eldabe, N. T., "Electrohydrodynamic Stability of Two Superposed Elasticoviscous Liquids in Plane Couette Flow", *Journal of Mathematical Physics*, Vol. 28, No. 11, pp. 2791–2800, 1987.

64. Wu, L. and S. Y. Chou, "Electrohydrodynamic Instability of a Thin Film of Viscoelastic Polymer Underneath a Lithographically Manufactured Mask", *Journal of non-Newtonian Fluid Mechanics*, Vol. 125, No. 2, pp. 91–99, 2005.

65. Roberts, S. A. and S. Kumar, "Electrohydrodynamic Instabilities in Thin Liquid Trilayer Films", *Physics of Fluids*, Vol. 22, No. 12, pp. 122102.1–15, 2010.

66. Ersoy, G. and A. K. Uguz, "Electro-Hydrodynamic Instability in a Microchannel between a Newtonian and a non-Newtonian Liquid", *Fluid Dynamics Research*, Vol. 44, No. 3, pp. 031406.1–12, 2012.

67. Nurocak, A. and A. K. Uguz, "Effect of the Direction of the Electric Field on the Interfacial Instability between a Passive Fluid and a Viscoelastic Polymer", *European Physical Journal Special Topics*, Vol. 219, No. 1, pp. 99–110, 2013.

68. Robinson, J. A., M. A. Bergougnou, G. P. Castle and I. I. Inculet, "The Electric Field at a Water Surface Stressed by an AC Voltage", *IEEE Transactions on Industry Applications*, Vol. 37, No. 3, pp. 735–742, 2001.

69. Narayanan, V. R. T., *Numerical Modeling of Microfluidic Two-Phase Electrohydrodynamic Instability*, Master's Thesis, New Brunswick Rutgers, The State University of New Jersey, January 2010.

70. Wray, A., D. Papageorgiou and O. Matar, "Electrostatically Controlled Large-Amplitude, Non-Axisymmetric Waves in thin Film Flows Down a Cylinder", *Jour-*

nal of Fluid Mechanics, Vol. 736, pp. R2.1–11, 2013.

71. Thaokar, R., "Oscillatory and Electrohydrodynamic Instabilities in Flow over a Viscoelastic Gel", *Sadhana*, Vol. 40, No. 3, pp. 1001–1022, 2015.

72. Castellanos, A. and A. González, "Nonlinear Electrohydrodynamics of Free Surfaces", *IEEE Transactions on Dielectrics and Electrical Insulation*, Vol. 5, pp. 334–343, 1998.

73. Johns, L. and R. Narayanan, *Interfacial Instability*, Springer-Verlag, New York, 2002.

74. Trefethen, L. N., *Spectral Methods in MATLAB*, Vol. 10, Siam, 2000.

75. Kutta, W., "Beitrag zur näherungweisen Integration totaler Differentialgleichungen", *Zeitschrift für Matematik und Physik*, Vol. 46, pp. 435–453, 1901.

76. Bockris, J. O. and A. K. Reddy, *Modern Electrochemistry 2B: Electrodics in Chemistry, Engineering, Biology and Environmental Science*, Vol. 2, Springer Science & Business Media, 2001.

APPENDIX A: DETAILS OF SCALING

In this section, the details of the derivation of the mathematical model are presented. The vectorial equations, e.g. the Navier-Stokes equation Equation 3.1, are shown in scalar forms. The determination of the characteristic scales denoted with overbars is also explained in this section. By letting the x-component and the z-component of the velocity u and w, respectively, the governing equations i.e., the x-component and the z-component of the Navier-Stokes equation, the continuity equation and the Laplace equation are written as

$$\rho u_t + \rho u u_x + \rho w u_z = -p_x + \mu(u_{xx} + u_{zz}) \tag{A.1}$$

$$\rho w_t + \rho u w_x + \rho w w_z = -p_z + \mu(w_{xx} + w_{zz}) \tag{A.2}$$

$$u_x + w_z = 0 \tag{A.3}$$

and

$$V_{xx} + V_{zz} = 0 \tag{A.4}$$

respectively. The length L and the width of the unstarred fluid d are selected as the characteristic length scales in the x-direction and the z-direction, respectively. Also, according to the lubrication theory

$$\frac{d}{L} = \epsilon << 1 \tag{A.5}$$

Then, to obtain a relation between the velocity scales, the continuity equation Equation A.3 is scaled as

$$\frac{\overline{u}}{L}\tilde{u}_{\tilde{x}} + \frac{\overline{w}}{d}\tilde{w}_{\tilde{z}} = 0 \tag{A.6}$$

and the velocity scales are related as

$$\overline{w} = \frac{d\overline{u}}{L} = \epsilon\overline{u} \tag{A.7}$$

Next, the time scale is determined via the kinematic condition:

$$\underline{v} \cdot \underline{n} = \underline{u} \cdot \underline{n} \tag{A.8}$$

By applying the dot product and using the definition of the normal vector given by Equation 3.13 and the surface speed $\underline{u} \cdot \underline{n}$, Equation A.8 becomes

$$\frac{-Z_x u + w}{(1 + Z_x^2)^{\frac{1}{2}}} = \frac{Z_t}{(1 + Z_x^2)^{\frac{1}{2}}} \tag{A.9}$$

and after the scaling it is written as

$$-\frac{d}{L}\overline{u}\tilde{Z}_{\tilde{x}}\tilde{u} + \frac{d}{L}\overline{u}\tilde{w} = \frac{d}{\overline{t}}\tilde{Z}_{\tilde{t}} \tag{A.10}$$

which gives the time scale as

$$\overline{t} = \frac{L}{\overline{u}} \tag{A.11}$$

Scaling the x-component of the Navier-Stokes equation, i.e., Equation A.1 gives

$$\rho\frac{\overline{u}^2}{L}(\tilde{u}_{\tilde{t}} + \tilde{u}\tilde{u}_{\tilde{x}} + \tilde{w}\tilde{u}_{\tilde{z}}) = -\frac{\overline{p}}{L}\tilde{p}_{\tilde{x}} + \mu(\frac{\overline{u}}{L^2}\tilde{u}_{\tilde{x}\tilde{x}} + \frac{\overline{u}}{L^2\epsilon^2}\tilde{u}_{\tilde{z}\tilde{z}}) \tag{A.12}$$

which yields the characteristic pressure scale as

$$\overline{p} = \frac{\mu \overline{u}}{L\epsilon^2} \tag{A.13}$$

Nondimensionalization of Equation A.12 gives

$$\epsilon^2 Re(\tilde{u}_{\tilde{t}} + \tilde{u}\tilde{u}_{\tilde{x}} + \tilde{w}\tilde{u}_{\tilde{z}}) = -\tilde{p}_{\tilde{x}} + \epsilon^2 \tilde{u}_{\tilde{x}\tilde{x}} + \tilde{u}_{\tilde{z}\tilde{z}} \tag{A.14}$$

where the Reynolds number Re emerges as

$$Re = \frac{\rho \overline{u} L}{\mu} \tag{A.15}$$

Scaling the z-component of the Navier-Stokes equation yields

$$\rho\epsilon \frac{\overline{u}^2}{L}(\tilde{w}_{\tilde{t}} + \tilde{u}\tilde{w}_{\tilde{x}} + \tilde{w}\tilde{w}_{\tilde{z}}) = -\frac{\mu\overline{u}}{L^2\epsilon^3}\tilde{p}_{\tilde{z}} + \frac{\mu\overline{u}}{L^2\epsilon}\tilde{w}_{\tilde{z}\tilde{z}} + \frac{\epsilon\mu\overline{u}}{L^2}\tilde{w}_{\tilde{x}\tilde{x}} \tag{A.16}$$

Equation A.16 written in dimensionless form as

$$\epsilon^4 Re(\tilde{w}_{\tilde{t}} + \tilde{u}\tilde{w}_{\tilde{x}} + \tilde{w}\tilde{w}_{\tilde{z}}) = -\tilde{p}_{\tilde{z}} + \epsilon^2 \tilde{w}_{\tilde{z}\tilde{z}} + \epsilon^4 \tilde{w}_{\tilde{x}\tilde{x}} \tag{A.17}$$

The Laplace equation is scaled as

$$\frac{\overline{V}}{d^2}\tilde{V}_{\tilde{z}\tilde{z}} + \frac{\overline{V}}{L^2}\tilde{V}_{\tilde{x}\tilde{x}} = 0 \tag{A.18}$$

where

$$\overline{V} = \Delta V \tag{A.19}$$

The nondimensionalized version of Equation A.18 is

$$\tilde{V}_{\tilde{z}\tilde{z}} + \epsilon^2 \tilde{V}_{\tilde{x}\tilde{x}} = 0 \tag{A.20}$$

The x-component of the Navier-Stokes equation for the starred fluid is given as

$$\rho^\star(u_t^\star + u^\star u_x^\star + w^\star u_z^\star) = -p_x^\star + \mu^\star(u_{xx}^\star + u_{zz}^\star) \tag{A.21}$$

Equation A.21 is scaled and nondimensionalized as

$$\rho^\star \frac{\overline{u}^2}{L}(\tilde{u}_{\tilde{t}}^\star + \tilde{u}^\star \tilde{u}_{\tilde{x}}^\star + \tilde{w}^\star \tilde{u}_{\tilde{z}}^\star) = -\frac{\mu\overline{u}}{\epsilon^2 L^2}\tilde{p}_{\tilde{x}}^\star + \mu^\star(\frac{\overline{u}}{L^2}\tilde{u}_{\tilde{x}\tilde{x}}^\star + \frac{\overline{u}}{\epsilon^2 L^2}\tilde{u}_{\tilde{z}\tilde{z}}^\star) \tag{A.22}$$

and

$$\epsilon^2 Re\frac{\phi}{\lambda}(\tilde{u}_{\tilde{t}}^\star + \tilde{u}^\star \tilde{u}_{\tilde{x}}^\star + \tilde{w}^\star \tilde{u}_{\tilde{z}}^\star) = -\frac{1}{\lambda}\tilde{p}_{\tilde{x}}^\star + \epsilon^2 \tilde{u}_{\tilde{x}\tilde{x}}^\star + \tilde{u}_{\tilde{z}\tilde{z}}^\star \tag{A.23}$$

respectively, where

$$\phi = \frac{\rho^\star}{\rho} \qquad \lambda = \frac{\mu^\star}{\mu} \tag{A.24}$$

The z-component of the Navier-Stokes equation for the starred fluid is given by

$$\rho^\star(w_t^\star + u^\star w_x^\star + w^\star w_z^\star) = -p_z^\star + \mu^\star(w_{xx}^\star + w_{zz}^\star) \tag{A.25}$$

Equation A.25 is scaled and nondimensionalized as

$$\rho^\star \epsilon \frac{\overline{u}^2}{L}(\tilde{w}_{\tilde{t}}^\star + \tilde{u}^\star \tilde{w}_{\tilde{x}}^\star + \tilde{w}^\star \tilde{w}_{\tilde{z}}^\star) = -\frac{\mu\overline{u}}{\epsilon^3 L^2}\tilde{p}_{\tilde{z}}^\star + \mu^\star(\frac{\epsilon\overline{u}}{L^2}\tilde{w}_{\tilde{x}\tilde{x}}^\star + \frac{\overline{u}}{\epsilon L^2}\tilde{w}_{\tilde{z}\tilde{z}}^\star) \tag{A.26}$$

and

$$\epsilon^4 Re\frac{\phi}{\lambda}(\tilde{w}_{\tilde{t}}^\star + \tilde{u}^\star \tilde{w}_{\tilde{x}}^\star + \tilde{w}^\star \tilde{w}_{\tilde{z}}^\star) = -\frac{1}{\lambda}\tilde{p}_{\tilde{z}}^\star + \epsilon^4 \tilde{w}_{\tilde{x}\tilde{x}}^\star + \epsilon^2 \tilde{w}_{\tilde{z}\tilde{z}}^\star \tag{A.27}$$

respectively. Next, the interface conditions are nondimensionalized. The dimensionless form of the scaled kinematic condition is given by

$$\tilde{u}\tilde{Z}_{\tilde{x}} + \tilde{w} = \tilde{Z}_{\tilde{t}} = \tilde{u}^{\star}\tilde{Z}_{\tilde{x}} + \tilde{w}^{\star} \tag{A.28}$$

By using the definitions of the normal and the tangent unit vectors given by Equation 3.12 and Equation 3.13, the no-slip condition Equation 3.7 is written as

$$u + Z_x w = u^{\star} + Z_x w^{\star} \tag{A.29}$$

The dimensionless form of Equation A.29 is

$$\tilde{u} + \epsilon^2 \tilde{Z}_{\tilde{x}}\tilde{w} = \tilde{u}^{\star} + \epsilon^2 \tilde{Z}_{\tilde{x}}\tilde{w}^{\star} \tag{A.30}$$

The double dot products of the electric and the fluid parts of the total stress tensor, Equation 3.15 and Equation 3.16 respectively, with the normal unit vector are

$$\underline{\underline{T}}^{F} : \underline{n}\,\underline{n} = -p + \frac{\mu}{1+Z_x^2}\left[2u_x\left(Z_x^2 - 1\right) - 2Z_x\left(u_z + w_x\right)\right] \tag{A.31}$$

and

$$\underline{\underline{T}}^{E} : \underline{n}\,\underline{n} = \frac{\varepsilon_0\varepsilon}{1+Z_x^2}\left[\frac{1}{2}\left(1 - Z_x^2\right)\left(V_z^2 - V_x^2\right) - 2Z_x V_x V_z\right] \tag{A.32}$$

Substituting Equation A.31 and Equation A.32 in Equation 3.8 gives

$$\begin{aligned}(p - p^{\star}) + \frac{\mu^{\star}}{1+Z_x^2}\left[2u_x^{\star}\left(Z_x^2 - 1\right) - 2Z_x\left(u_z^{\star} + w_x^{\star}\right)\right] \\ + \frac{\varepsilon_0\varepsilon^{\star}}{1+Z_x^2}\left[\frac{1}{2}\left(1 - Z_x^2\right)\left(V_z^{\star 2} - V_x^{\star 2}\right) - 2Z_x V_x^{\star} V_z^{\star}\right] \\ - \frac{\mu}{1+Z_x^2}\left[2u_x\left(Z_x^2 - 1\right) - 2Z_x\left(u_z + w_x\right)\right] \\ - \frac{\varepsilon_0\varepsilon}{1+Z_x^2}\left[\frac{1}{2}\left(1 - Z_x^2\right)\left(V_z^2 - V_x^2\right) - 2Z_x V_x V_z\right] + \frac{\gamma Z_{xx}}{\left(1+Z_x^2\right)^{\frac{3}{2}}} = 0\end{aligned} \tag{A.33}$$

Scaling and nondimensionalization yields

$$\begin{aligned}\frac{\mu\overline{u}}{L\epsilon^2}\left(\tilde{p}-\tilde{p}^\star\right)+\frac{\mu^\star}{1+\epsilon^2\tilde{Z}_{\tilde{x}}^2}\frac{\overline{u}}{L}\left[2\tilde{u}_{\tilde{x}}^\star\left(\epsilon^2\tilde{Z}_{\tilde{x}}^2-1\right)-2\tilde{Z}_{\tilde{x}}\left(\tilde{u}_{\tilde{z}}^\star+\epsilon^2\tilde{w}_{\tilde{x}}^\star\right)\right]\\ +\frac{\varepsilon_0\varepsilon^\star\Delta V^2}{1+\epsilon^2\tilde{Z}_{\tilde{x}}^2}\frac{1}{L^2}\left[\frac{1}{2}\left(1-\epsilon^2\tilde{Z}_{\tilde{x}}^2\right)\left(\frac{1}{\epsilon^2}\tilde{V}_{\tilde{z}}^{\star 2}-\tilde{V}_{\tilde{x}}^{\star 2}\right)-2\tilde{Z}_{\tilde{x}}\tilde{V}_{\tilde{x}}^\star\tilde{V}_{\tilde{z}}^\star\right]\\ -\frac{\mu}{1+\epsilon^2\tilde{Z}_{\tilde{x}}^2}\frac{\overline{u}}{L}\left[2\tilde{u}_{\tilde{x}}\left(\epsilon^2\tilde{Z}_{\tilde{x}}^2-1\right)-2\tilde{Z}_{\tilde{x}}\left(\tilde{u}_{\tilde{z}}+\epsilon^2\tilde{w}_{\tilde{x}}\right)\right]\\ -\frac{\varepsilon_0\varepsilon^\star\Delta V^2}{1+\epsilon^2\tilde{Z}_{\tilde{x}}^2}\frac{1}{L^2}\left[\frac{1}{2}\left(1-\epsilon^2\tilde{Z}_{\tilde{x}}^2\right)\left(\frac{1}{\epsilon^2}\tilde{V}_{\tilde{z}}^2-\tilde{V}_{\tilde{x}}^2\right)-2\tilde{Z}_{\tilde{x}}\tilde{V}_{\tilde{x}}\tilde{V}_{\tilde{z}}\right]\\ +\frac{\gamma\epsilon}{L}\frac{\tilde{Z}_{\tilde{x}\tilde{x}}}{\left(1+\epsilon^2\tilde{Z}_{\tilde{x}}^2\right)^{\frac{3}{2}}}=0\end{aligned}\tag{A.34}$$

and

$$\begin{aligned}\left(\tilde{p}-\tilde{p}^\star\right)+\frac{\lambda\epsilon^2}{1+\epsilon^2\tilde{Z}_{\tilde{x}}^2}\left[2\tilde{u}_{\tilde{x}}^\star\left(\epsilon^2\tilde{Z}_{\tilde{x}}^2-1\right)-2\tilde{Z}_{\tilde{x}}\left(\tilde{u}_{\tilde{z}}^\star+\epsilon^2\tilde{w}_{\tilde{x}}^\star\right)\right]\\ +Eb\frac{\varepsilon^\star}{1+\epsilon^2\tilde{Z}_{\tilde{x}}^2}\left[\frac{1}{2}\left(1-\epsilon^2\tilde{Z}_{\tilde{x}}^2\right)\left(\tilde{V}_{\tilde{z}}^{\star 2}-\epsilon^2\tilde{V}_{\tilde{x}}^{\star 2}\right)-\epsilon^2\tilde{Z}_{\tilde{x}}\tilde{V}_{\tilde{x}}^\star\tilde{V}_{\tilde{z}}^\star\right]\\ -\frac{\epsilon^2}{1+\epsilon^2\tilde{Z}_{\tilde{x}}^2}\left[2\tilde{u}_{\tilde{x}}\left(\epsilon^2\tilde{Z}_{\tilde{x}}^2-1\right)-2\tilde{Z}_{\tilde{x}}\left(\tilde{u}_{\tilde{z}}+\epsilon^2\tilde{w}_{\tilde{x}}\right)\right]\\ -Eb\frac{\varepsilon}{1+\epsilon^2\tilde{Z}_{\tilde{x}}^2}\left[\frac{1}{2}\left(1-\epsilon^2\tilde{Z}_{\tilde{x}}^2\right)\left(\tilde{V}_{\tilde{z}}^2-\epsilon^2\tilde{V}_{\tilde{x}}^2\right)-\epsilon^2\tilde{Z}_{\tilde{x}}\tilde{V}_{\tilde{x}}\tilde{V}_{\tilde{z}}\right]\\ +\frac{\epsilon^3}{Ca}\frac{\tilde{Z}_{\tilde{x}\tilde{x}}}{\left(1+\epsilon^2\tilde{Z}_{\tilde{x}}^2\right)^{\frac{3}{2}}}=0\end{aligned}\tag{A.35}$$

where

$$Eb=\frac{\varepsilon_0\Delta V^2}{\mu\overline{u}L}\qquad Ca=\frac{\mu\overline{u}}{\gamma}\tag{A.36}$$

The double dot product of the total stress tensor by the normal and the tangential unit vector is

$$\left(\underline{E}\,\underline{E}-\frac{1}{2}|\underline{E}|^2\underline{\underline{I}}\right):\underline{n}\,\underline{t}=\left[\frac{1}{1+Z_x^2}\left(V_x+Z_xV_z\right)\left(-V_xZ_x+V_z\right)\right]\tag{A.37}$$

$$\mu\left(\nabla\underline{v}+(\nabla\underline{v})^t\right):\underline{n}\,\underline{t}=\frac{\mu}{1+Z_x^2}\left[-4Z_xu_x+(w_x+u_z)\left(1-Z_x^2\right)\right] \tag{A.38}$$

and

$$-p\underline{\underline{I}}:\underline{n}\,\underline{t}=0 \tag{A.39}$$

Combining Equation 3.9 and Equations A.37 to A.39 gives

$$\begin{aligned}\frac{\mu}{1+Z_x^2}\left[-4Z_xu_x+(w_x+u_z)\left(1-Z_x^2\right)\right]+\left[\frac{\varepsilon_0\varepsilon}{1+Z_x^2}\left(V_x+Z_xV_z\right)\left(-V_xZ_x+V_z\right)\right]\\ =\frac{\mu^\star}{1+Z_x^2}\left[-4Z_xu_x^\star+(w_x^\star+u_z^\star)\left(1-Z_x^2\right)\right]\\ +\left[\frac{\varepsilon_0\varepsilon^\star}{1+Z_x^2}\left(V_x^\star+Z_xV_z^\star\right)\left(-V_x^\star Z_x+V_z^\star\right)\right]\end{aligned} \tag{A.40}$$

which is scaled and written in dimensionless form as

$$\begin{aligned}\frac{\mu\overline{u}}{L}\left[-4\epsilon^2\tilde{Z}_{\tilde{x}}\tilde{u}_{\tilde{x}}+\left(\epsilon^2\tilde{w}_{\tilde{x}}+\tilde{u}_{\tilde{z}}\right)\left(1-\epsilon^2\tilde{Z}_{\tilde{x}}^2\right)\right]+\left[\frac{\varepsilon_0\varepsilon\Delta V^2}{L^2}\left(\tilde{V}_{\tilde{x}}+\tilde{Z}_{\tilde{x}}\tilde{V}_{\tilde{z}}\right)\left(-\epsilon^2\tilde{V}_{\tilde{x}}\tilde{Z}_{\tilde{x}}+\tilde{V}_{\tilde{z}}\right)\right]\\ =\frac{\mu^\star\overline{u}}{L}\left[-4\epsilon^2\tilde{Z}_{\tilde{x}}\tilde{u}_{\tilde{x}}^\star+\left(\epsilon^2\tilde{w}_{\tilde{x}}^\star+\tilde{u}_{\tilde{z}}^\star\right)\left(1-\epsilon^2\tilde{Z}_{\tilde{x}}^2\right)\right]\\ +\left[\frac{\varepsilon_0\varepsilon\Delta V^2}{L^2}\left(\tilde{V}_{\tilde{x}}^\star+\tilde{Z}_{\tilde{x}}\tilde{V}_{\tilde{z}}^\star\right)\left(-\epsilon^2\tilde{V}_{\tilde{x}}^\star\tilde{Z}_{\tilde{x}}+\tilde{V}_{\tilde{z}}^\star\right)\right]\end{aligned} \tag{A.41}$$

and

$$\begin{aligned}\left[-4\epsilon^2\tilde{Z}_{\tilde{x}}\tilde{u}_{\tilde{x}}+\left(\epsilon^2\tilde{w}_{\tilde{x}}+\tilde{u}_{\tilde{z}}\right)\left(1-\epsilon^2\tilde{Z}_{\tilde{x}}^2\right)\right]-\lambda\left[-4\epsilon^2\tilde{Z}_{\tilde{x}}\tilde{u}_{\tilde{x}}^\star+\left(\epsilon^2\tilde{w}_{\tilde{x}}^\star+\tilde{u}_{\tilde{z}}^\star\right)\left(1-\epsilon^2\tilde{Z}_{\tilde{x}}^2\right)\right]\\ +Eb\,\varepsilon\left[\left(\tilde{V}_{\tilde{x}}+\tilde{Z}_{\tilde{x}}\tilde{V}_{\tilde{z}}\right)\left(-\epsilon^2\tilde{V}_{\tilde{x}}\tilde{Z}_{\tilde{x}}+\tilde{V}_{\tilde{z}}\right)\right]-\\ Eb\,\varepsilon^\star\left[\left(\tilde{V}_{\tilde{x}}^\star+\tilde{Z}_{\tilde{x}}\tilde{V}_{\tilde{z}}^\star\right)\left(-\epsilon^2\tilde{V}_{\tilde{x}}^\star\tilde{Z}_{\tilde{x}}+\tilde{V}_{\tilde{z}}^\star\right)\right]=0\end{aligned} \tag{A.42}$$

respectively. The continuity of the electric field Equation 3.18 is written in scalar form as

$$V_x+V_zZ_x=V_x^\star+V_z^\star Z_x \tag{A.43}$$

$$\frac{\overline{V}}{L}V_x + \frac{\overline{V}}{L}V_z Z_x = \frac{\overline{V}}{L}V_x^\star + \frac{\overline{V}}{L}V_z^\star Z_x \tag{A.44}$$

Equation A.44 is written in the dimensionless form as

$$\tilde{V}_{\tilde{x}} + \tilde{V}_{\tilde{z}}\tilde{Z}_{\tilde{x}} = \tilde{V}_{\tilde{x}}^\star + \tilde{V}_{\tilde{z}}^\star \tilde{Z}_{\tilde{x}} \tag{A.45}$$

The Gauss's law Equation 3.19 can be written as

$$q = \frac{1}{(1+Z_x^2)^{\frac{1}{2}}}\left(\varepsilon_0\varepsilon^\star(Z_x V_x^\star - V_z^\star) - \varepsilon_0\varepsilon(Z_x V_x - V_z)\right) \tag{A.46}$$

Scaling Equation A.46 yields

$$\overline{q}\tilde{q} = \frac{1}{(1+\epsilon^2 Z_x^2)^{\frac{1}{2}}}\left(\varepsilon_0\varepsilon^\star(\epsilon\frac{\overline{V}}{L}\tilde{Z}_{\tilde{x}}\tilde{V}_{\tilde{x}}^\star - \frac{\overline{V}}{d}\tilde{V}_{\tilde{z}}^\star) - \varepsilon_0\varepsilon(\epsilon\frac{\overline{V}}{L}\tilde{Z}_{\tilde{x}}\tilde{V}_{\tilde{x}} - \frac{\overline{V}}{d}\tilde{V}_{\tilde{z}})\right) \tag{A.47}$$

By letting

$$\overline{q} = \frac{\varepsilon_0\Delta V}{d} \tag{A.48}$$

Equation A.47 is given in dimensionless form as

$$\tilde{q} = \frac{1}{(1+\epsilon^2 Z_x^2)^{\frac{1}{2}}}\left(\varepsilon^\star(\epsilon^2\tilde{Z}_{\tilde{x}}\tilde{V}_{\tilde{x}}^\star - \tilde{V}_{\tilde{z}}^\star) - \varepsilon(\epsilon^2\tilde{Z}_{\tilde{x}}\tilde{V}_{\tilde{x}} - \tilde{V}_{\tilde{z}})\right) \tag{A.49}$$

The charge conservation Equation 3.20 yields

$$\begin{aligned} q_t - \frac{Z_t Z_x}{1+Z_x^2}q_x + \frac{1}{(1+Z_x^2)^2}\left(\frac{u+wZ_x}{(1+Z_x^2)^2}q\right)_x + Z_{xx}\frac{w-uZ_x}{(1+Z_x^2)^2}q \\ = \frac{\sigma}{(1+Z_x^2)^{\frac{1}{2}}}(Z_x V_x - V_z) - \frac{\sigma^\star}{(1+Z_x^2)^{\frac{1}{2}}}(Z_x V_x^\star - V_z^\star) \end{aligned} \tag{A.50}$$

Equation A.50 is scaled and made dimensionless as

$$\overline{q}\frac{\overline{u}}{L}\left[\tilde{q}_{\tilde{t}}-\epsilon^2\frac{\tilde{Z}_{\tilde{t}}\tilde{Z}_{\tilde{x}}}{(1+\epsilon^2\tilde{Z}_{\tilde{x}}^2)}\tilde{q}_{\tilde{x}}+\frac{1}{(1+\epsilon^2\tilde{Z}_{\tilde{x}}^2)^{\frac{1}{2}}}\left(\frac{\tilde{u}+\epsilon^2\tilde{w}\tilde{Z}_{\tilde{x}}}{(1+\epsilon^2\tilde{Z}_{\tilde{x}}^2)^2}\tilde{q}\right)_{\tilde{x}}+\epsilon^2\tilde{Z}_{\tilde{x}\tilde{x}}\frac{\tilde{w}-\tilde{u}\tilde{Z}_{\tilde{x}}}{(1+\epsilon^2\tilde{Z}_{\tilde{x}}^2)^2}\tilde{q}\right]$$
$$=\frac{1}{(1+\epsilon^2\tilde{Z}_{\tilde{x}}^2)^{\frac{1}{2}}}\frac{\Delta V}{L}\left[\sigma\left(\epsilon\tilde{Z}_{\tilde{x}}\tilde{V}_{\tilde{x}}-\frac{1}{\epsilon}\tilde{V}_{\tilde{z}}\right)-\sigma^\star\left(\epsilon\tilde{Z}_{\tilde{x}}\tilde{V}_{\tilde{x}}^\star-\frac{1}{\epsilon}\tilde{V}_{\tilde{z}}^\star\right)\right] \quad \text{(A.51)}$$

and

$$\tilde{q}_{\tilde{t}}-\epsilon^2\frac{\tilde{Z}_{\tilde{t}}\tilde{Z}_{\tilde{x}}}{(1+\epsilon^2\tilde{Z}_{\tilde{x}}^2)}\tilde{q}_{\tilde{x}}+\frac{1}{(1+\epsilon^2\tilde{Z}_{\tilde{x}}^2)^{\frac{1}{2}}}\left(\frac{\tilde{u}+\epsilon^2\tilde{w}\tilde{Z}_{\tilde{x}}}{(1+\epsilon^2\tilde{Z}_{\tilde{x}}^2)^2}\tilde{q}\right)_{\tilde{x}}+\epsilon^2\tilde{Z}_{\tilde{x}\tilde{x}}\frac{\tilde{w}-\tilde{u}\tilde{Z}_{\tilde{x}}}{(1+\epsilon^2\tilde{Z}_{\tilde{x}}^2)^2}\tilde{q}$$
$$=S\frac{1}{(1+\epsilon^2\tilde{Z}_{\tilde{x}}^2)^{\frac{1}{2}}}\left[\left(\epsilon^2\tilde{Z}_{\tilde{x}}\tilde{V}_{\tilde{x}}-\tilde{V}_{\tilde{z}}\right)-\alpha\left(\epsilon^2\tilde{Z}_{\tilde{x}}\tilde{V}_{\tilde{x}}^\star-\tilde{V}_{\tilde{z}}^\star\right)\right] \quad \text{(A.52)}$$

respectively, where

$$S=\frac{L\sigma}{\varepsilon_0\overline{u}} \qquad and \qquad \alpha=\frac{\sigma^\star}{\sigma} \quad \text{(A.53)}$$

Finally using Equation A.45 and Equation A.49, the tangential stress balance Equation A.42 is simplified as

$$\left[-4\epsilon^2\tilde{Z}_{\tilde{x}}\tilde{u}_{\tilde{x}}+\left(\epsilon^2\tilde{w}_{\tilde{x}}+\tilde{u}_{\tilde{z}}\right)\left(1-\epsilon^2\tilde{Z}_{\tilde{x}}^2\right)\right]-\lambda\left[-4\epsilon^2\tilde{Z}_{\tilde{x}}\tilde{u}_{\tilde{x}}^\star+\left(\epsilon^2\tilde{w}_{\tilde{x}}^\star+\tilde{u}_{\tilde{z}}^\star\right)\left(1-\epsilon^2\tilde{Z}_{\tilde{x}}^2\right)\right]$$
$$Eb\,\tilde{q}\left(1+\epsilon^2\tilde{Z}_{\tilde{x}}^2\right)^{\frac{1}{2}}\left(\tilde{V}_{\tilde{x}}+\tilde{Z}_{\tilde{x}}\tilde{V}_{\tilde{z}}\right)=0 \quad \text{(A.54)}$$

The velocity scale $\overline{u}$ is selected as the interface speed at the base state U.